Structure-Activity Relationship of Neuroactive Steroids, Midazolam, and Perampanel Toward Mitigating Tetramine-Triggered Activity in Murine Hippocampal Neuronal Networks

Shane Antrobus,* Brandon Pressly,[†] Atefeh Mousavi Nik,* Heike Wulff,[†] and Isaac N. Pessah [ID]*,[1]

*Department of Molecular Biosciences, School of Veterinary Medicine, University of California, Davis, Davis, California 95616, USA; and [†]Department of Pharmacology, School of Medicine, University of California, Davis, Davis, California 95616, USA

[1]To whom correspondence should be addressed at Department of Molecular Biosciences, School of Veterinary Medicine, University of California, Davis, 1089 Veterinary Medicine Drive, Davis, CA 95616, USA. E-mail: inpessah@ucdavis.edu.

ABSTRACT

Tetramethylenedisulfotetramine (tetramine or TETS), a potent convulsant, triggers abnormal electrical spike activity (ESA) and synchronous Ca^{2+} oscillation (SCO) patterns in cultured neuronal networks by blocking gamma-aminobutyric acid ($GABA_A$) receptors. Murine hippocampal neuronal/glial cocultures develop extensive dendritic connectivity between glutamatergic and GABAergic inputs and display two distinct SCO patterns when imaged with the Ca^{2+} indicator Fluo-4: Low amplitude SCO events (LASE) and High amplitude SCO events (HASE) that are dependent on TTX-sensitive network electrical spike activity (ESA). Acute TETS ($3.0\,\mu M$) increased overall network SCO amplitude and decreased SCO frequency by stabilizing HASE and suppressing LASE while increasing ESA. In multielectrode arrays, TETS also increased burst frequency and synchronicity. In the presence of TETS ($3.0\,\mu M$), the clinically used anticonvulsive perampanel ($0.1–3.0\,\mu M$), a noncompetitive AMPAR antagonist, suppressed all SCO activity, whereas the $GABA_A$ receptor potentiator midazolam (1.0-$30\,\mu M$), the current standard of care, reciprocally suppressed HASE and stabilized LASE. The neuroactive steroid (NAS) allopregnanolone ($0.1–3.0\,\mu M$) normalized TETS-triggered patterns by selectively suppressing HASE and increasing LASE, a pharmacological pattern distinct from its epimeric form eltanolone, ganaxolone, alphaxolone, and XJ-42, which significantly potentiated TETS-triggered HASE in a biphasic manner. Cortisol failed to mitigate TETS-triggered patterns and at $>1\,\mu M$ augmented them. Combinations of allopregnanolone and midazolam were significantly more effective at normalizing TETS-triggered SCO patterns, ESA patterns, and more potently enhanced GABA-activated Cl^- current, than either drug alone.

Key words: acute neurotoxicity; benzodiazepines; calcium signaling; neuroactive steroids; neuronal networks; pesticides; seizure; tetramine.

Tetramethylenedisulfotetramine (2,6-dithia-1,3,5,7-tetraazaa-damantane 2,2,6,6-tetraoxide, tetramine or TETS) is a potent neuroexcitatory toxicant that was historically used as a rodenticide (Lauková *et al.*, 2020). TETS is odorless and tasteless, easy to synthesize from common starting materials and stable in aqueous solutions. Because of its chemical properties, ease of

Impact Statement

The results identify differential patterns of activity of NAS toward TETS-triggered seizure-like activity that likely reflect their differential activities toward synaptic and extra synaptic GABA$_A$ receptors as well as Ca^{2+}-regulatory mechanisms within hippocampal neuronal networks *in vitro*.

synthesis and its exquisite neurotoxicity (LD$_{50}$ value of 0.1–0.3 mg/kg for mammals), TETS is considered a chemical threat agent (Barrueto *et al.*, 2003a; Whitlow *et al.*, 2005; Zhang *et al.*, 2011). Although all commercial and household uses of TETS have been banned worldwide, it has continued to be produced and used illicitly, mainly in China (Barrueto *et al.*, 2003b; Jett and Spriggs, 2018; Patocka, *et al.*, 2018). Sublethal doses of TETS have been reported to produce electrographic seizures and neuronal network depolarization with symptoms of hyperactivity, restlessness, headache, dizziness and vomiting (Li *et al.*, 2014). Higher doses of TETS result in the onset of seizures that progress rapidly to status epilepticus and death, if untreated (Croddy, 2004; Whitlow *et al.*, 2005; Zhang *et al.*, 2011; Zhu *et al.*, 2004). The lethal dose for humans has been estimated at 7–10 mg.

TETS is classified as a cage convulsant based on its tretraazatricyclic ring structure, which is chemically stable and resistant to metabolism. TETS crosses the blood-brain barrier after exposure (Pressly *et al.*, 2020), resulting in a dramatic imbalance of excitation/inhibition of neural circuits across brain regions that can elicit status epilepticus (Zhu *et al.*, 2004). Acute effects of TETS are mediated by its ability to block chloride (Cl$^-$) inward currents carried by ionotropic gamma-aminobutyric acid receptors (GABA$_A$R) comprised heteropentamers with the general stoichiometry $2\alpha_x2\beta_x\gamma_x$ (Rudolph and Knoflach, 2011; Zhao *et al.*, 2014). GABA$_A$R are localized at synaptic, extrasynaptic, as well as somatic and axonal regions of neurons, where they provide inhibitory inputs essential for maintaining the balance of excitation-inhibition within local and long-range central neuronal circuits (Moult, 2009; Niquet *et al.*, 2016). The 19 genes that encode subunits for GABA$_A$R, which can be distributed broadly among axo-somato-dendritic membranes, provide an enormous diversity in the repertoire of negative regulation at several levels of brain circuitry (Nusser, 2016). In this regard, TETS was recently reported to be particularly potent at blocking GABA-activated chloride currents measured from cells expressing $\alpha_2\beta_3\gamma_2$ (IC$_{50}$ 480 nM) and $\alpha_6\beta_3\gamma_2$ (IC$_{50}$ 400 nM) GABA$_A$ receptor subunit combinations, whereas $\alpha_4\beta_3\delta$ and $\alpha_6\beta_3\delta$ subunit combinations were less sensitive to TETS (IC$_{50}$ 3.0 and 3.7 μM, respectively; Pressly *et al.*, 2018). This structure-activity profile is distinct from that of picrotoxinin, the active component of picrotoxin.

In vitro assays using potentiometric dyes that report changes in membrane potential of cell lines expressing defined GABA$_A$R subunit compositions have provided a convenient means to perform rapid-throughput screening to identify compounds that are blockers, direct activators, and allosteric potentiators, and to characterize receptor interactions using automated multi-well plate readers, such as FLIPR TETRA (Falk-Petersen *et al.*, 2017; Nik *et al.*, 2017). Results from plate-based potentiometric approaches are useful and convenient for identifying new chemical entities and defining detailed structure activity relationships (SARs) among GABA$_A$R subtypes, especially since they appear to have good predictive fidelity when compared with results from more time-intensive whole-cell voltage-clamp approaches. However, approaches using recombinantly expressed receptors do not recapitulate the spatial complexity of GABA$_A$R subunit expression found within neuronal networks and their contributions to the negative control of excitatory neurotransmission, such as those afforded by experiments with acutely prepared brain slices and dissociated neuronal/glial cocultures. With regard to the latter approach, distinct, though interrelated, physiological parameters of primary neuronal/glial cocultures can be quantitatively measured with two relatively rapid-throughput assays: (1) Ca^{2+} sensitive indicators can be used to detect patterns of spontaneous synchronous Ca^{2+} oscillations (SCOs), and (2) multi-well electrode arrays can be used to measure patterns of electrical spike activity (ESA).

GABA$_A$R blockers, such as TETS (Cao *et al.*, 2012a, 2017) and other seizure inducing compounds such as the K$^+$ channel blocker 4-aminopyridine and the muscarinic agonist pilocarpine, produce distinguishable changes in patterns of SCOs and/or ESA (Bradley and Strock, 2019; Bradley *et al.*, 2018; Cao *et al.*, 2015; Frank *et al.*, 2017; Leinekugel *et al.*, 1997; McConnell *et al.*, 2012; Tukker *et al.*, 2018). Thus, SCO and ESA patterns are useful and convenient tools to identify seizurogenic agents of diverse functional mechanism(s) and have shown value in the discovery of novel antiseizure intervention strategies, as demonstrated for TETS (Bruun *et al.*, 2015; Cao *et al.*, 2012a; Pessah *et al.*, 2016).

Rapid throughput *in vitro* assays using neuronal networks that develop a high degree of connectivity have predictive value for prioritizing novel therapeutic strategies that evaluate seizure mitigation efficacy *in vivo*, especially against potent threat agents that directly block GABA$_A$R and overexcite the central nervous system. Here, we used measures of SCO and ESA patterns to analyze five neuroactive steroids (NASs) shown to be positive allosteric modulators (PAMs) and cortisol, a negative control, in the absence and presence of the benzodiazepine midazolam (MDZ) to directly compare their potential to mitigate TETS-triggered abnormalities in neuronal network activity patterns. We identified that NASs produced distinct influences toward reversing abnormal SCO and electrical spike patterns triggered by TETS and identify allopregnanolone (ALLO) as a particularly efficacious candidate for restoring control patterns of activity. Our experiments further indicate significant therapeutic benefit of combinatorial therapy with NAS and MDZ to treat acute hyperexcitability triggered by TETS.

MATERIALS AND METHODS

Chemicals. TETS was synthesized and purified to >99% as previously described (Zolkowska *et al.*, 2012). XJ-42 ((3α,5α,20E)-3-hydroxy-13,24-cyclo-18-norcholan-20-ene-21-carbonitrile) was a generous gift of Dr Douglas F. Covey (Washington University School of Medicine, St Louis, Missouri; Covey and Jiang, 2014). ALLO (3α-hydroxy-5α-pregnan-20-one) was custom synthesized by SAFC Pharma (Madison, Wisconsin).

Tocris (Minneapolis, Minnesota) was the source of alphaxalone (ALPHAX; (3α,5α)-3-hydroxypregnane-11,20-dione), and ganaxolone (GANAX; (3α,5α)-3-hydroxy-3-methyl-pregnan-20-one), eltanolone (ELTAN; 3α-hydroxy-5β-pregnan-20-one),

cortisol (11β,17α,21-trihydroxypregn-4-ene-3,20-dione), midazolam (MDZ), and tetrodotoxin (TTX) citrate. Perampanel (PERAMP; 3-(2-cyanophenyl)-5-(2-pyridyl)-1-phenyl-1,2-dihydropyridin-2-one) was purchased from Sigma Aldrich (St Louis, Missouri). All purchased reagents were >97% purity. The structures of the compounds tested are given in Supplementary Figure 1.

Animals. All collections of mouse tissues from wildtype C57BL/6J mice (origin The Jackson Laboratory; Bar Harbor, Maine) for the studies were conducted using protocols approved by the Institutional Animal Care and Use Committee (IACUC No. 18094) at the University of California at Davis (Davis, California). All animals were maintained in a vivarium with constant temperature and humidity with a 12:12 h light-dark cycle. Animals were provided with Mouse Diet 20 (PicoLab) and autoclaved drinking water by the UC Davis animal facility *ad libitum*.

Coculture of primary murine hippocampal neuronal/glial cells. Hippocampal neuronal/glial cultures were obtained from C57BL/6J mouse pups at postnatal day 0–1. The brains from male and female pups were combined for establishing cultures. Dissociated hippocampal neurons were plated in poly-L-lysine-coated, clear-bottomed, black walled 96-well imaging plates (BD, Franklin Lakes, New Jersey) at a density of 75 000 cells/well in complete Neurobasal medium (ThermoFisher, Waltham, Massachusetts) supplemented with 0.5 mM L-glutamine, GS21 supplement (Cat No. GSM-3100; MTI-GlobalStem Products, ThermoFisher, Gaithersburg, Maryland), 10 mM HEPES with 5% fetal bovine serum (FBS) (Atlanta Biologicals, Norcross, Georgia) for measurements on FLIPR TETRA. FBS concentration was reduced to 2.5% in the first day and halved at each change of media. For microelectrode array assays, 110 000 cells/well were seeded in a 12-well Maestro plate (Axion BioSystems, Atlanta, Georgia). Cytosine arabinoside (5 μM; Sigma Aldrich, St Louis, Missouri) was added to all cultures at 2 days *in vitro* (DIV) and half of the media was changed every 3–4 days (the cytosine arabinoside concentration halved at each change of media). Neurons were incubated at 37°C with 5% CO_2 and 95% humidity for 14–16 days.

Immunocytochemistry. Hippocampal cultures were fixed with 4% paraformaldehyde in PBS (pH 7.4) for 15 min. Cells were permeabilized with 0.1% Triton X-100 in PBS for 5 min. Cultures were then incubated for 1 h in blocking solution (10% goat serum, 0.1% Tween 20 in PBS) at room temperature. Next, cultures were incubated overnight at 4°C with primary antibodies diluted in blocking solution. The following 4 pairs of primary and secondary antibody were used: (1) chicken anti-microtubule-associated protein-2 (anti-MAP2; 1:1000, Thermo Fisher, PA1-16751)/goat antichicken Alexa 488 (1:1000, Invitrogen, Carlsbad, California, A-11039); (2) mouse monoclonal anit-glial fibrilary acidic protein (anti-GFAP; 1:500, Cell Signaling Technologies, Danvers, Massachusetts, 3670S)/antimouse IgG Alexa 555 (1:1000, Cell Signaling Technologies, 4409); (3) rabbit antivesicular GABA transporters VGATs; 1:500, Synaptic Systems, 131 003)/goat anti-rabbit Alexa 546 (1:1000, Invitrogen, A-11035); and (4) guinea pig antivesicular glutamate transporters (VGLUT1; 1:500, Synaptic Systems, Göttingen, Germany, 135 304)/goat antiguinea pig Alexa 647 (1:1000, Invitrogen, A-21450). On the following day, cultures were washed and treated with secondary antibodies diluted in blocking solution for 2 h at room temperature, then incubated for 5 min with NucBlue (Hoechst 33342; 2′-[4-ethoxyphenyl]-5-[4-methyl-1-piperazinyl]-2,5′-bi-1H-benzimidazole) nuclear stain (Molecular Probes, Eugene, Oregon) diluted in PBS (2 drops/ml) followed by washing with PBS. Images were collected and processed using an ImageXpress Micro high-content imaging system and associated software (Molecular Devices, San Jose, California).

Vesicular GABA transporters cellular imaging assay. Neuronal/glial cocultures prepared from postnatal day 0–1 murine hippocampus form elaborate dendritic architectures with a high degree of synaptic connectivity. They display SCOs by 6 DIV with frequency and amplitude patterns that transition from predominantly low frequency, high amplitude events to more complex patterns by 16 DIV (Cao et al., 2017). Therefore, the present study focused on the acute influence of TETS and the degree to which subsequent therapeutic candidates restore SCO patterns to baseline recording using cultures between 14 and 16 DIV. Because the FLIPR TETRA plate reader platform measures and records intracellular Ca^{2+} transients from 96-wells simultaneously, responses from each well to TETS or drug were compared with their own baseline activity. More specifically, the culture medium was removed on the day of each experiment, and 65 μl of prewarmed (37°C) Locke's buffer (NaCl 154 mM, KCl 5.6 mM, $CaCl_2$ 2.3 mM, $MgCl_2$ 1 mM, HEPES 8.6 mM, glucose 5.6 mM, glycine 0.0001 mM, and pH 7.4), 0.5 mg/ml bovine serum albumin fraction V (Fisher Scientific), and 0.0005 mM Ca^{2+} fluorescence dye Fluo-4-AM (Sigma-Aldrich) were immediately added to each well. Plates were returned to the culture incubator for 1 h at 37°C. Next, cells were gently washed with Locke's buffer 3 times and permitted to equilibrate for 10–15 min. Baseline SCO recordings were taken for 10 min. Then the programmable 96-channel pipetting robotic system added 3 μM TETS to the wells, and changes in SCO patterns were monitored for an additional 20 min to record the phase I response (a rapid but transient elevation in cytoplasmic Ca^{2+}) and phase II responses (sustained alteration in frequency and amplitude of SCO patterns) as previously described by us (Cao et al., 2012a). Therapeutic candidates (or vehicle, 0.01% dimethylsulfoxide, DMSO) were added, either in the absence or subsequent to the addition of TETS at 7× concentration from the source plate as indicated in each figure protocol. The potency and efficacy of therapeutic candidates to normalized TETS-triggered patterns were tested with the following protocol: Baseline recording (10 min)—TETS recording (10 min)—TETS + therapeutic candidate (10 min). The last 5 min of data recorded from each of the wells (TETS, vehicle, and/or drug therapeutic candidate) were used to analyze phase II response amplitude and frequency parameters normalized to vehicle control for statistical comparison to vehicle and TETS alone during the same timeframe of data acquisition. IC_{50} or EC_{50} were calculated using nonlinear curve fitting where indicated.

Specifically, ScreenWorks Peak Pro Software (Version 3.2; San Jose, California) was used to normalize the magnitude of SCOs based on $(F_{max} - F_{min})/F_{min}$, where F_{max} was the peak for each spike, and F_{min} was the baseline just prior to the spike. *Kinetic Reduction Configuration* was used to score frequency and amplitude of SCOs. Total SCO frequency was scored using *Peak Frequency (BPM)* with *Configure Peak Detection* settings: smooth width 1, fit width 3, slope threshold 0.01, amplitude threshold dynamic 7. High amplitude SCO events (HASE) spike frequency was scored using *Peak Frequency (BPM)* with *Configure Peak Detection* settings: smooth width 1, fit width 3, slope threshold 0.01, amplitude threshold dynamic 75. These settings resulted

in binning HASE at $\Delta F/F0 > 0.3$. Low amplitude SCO event (LASE) spike frequency was calculated by subtracting HASE frequency from total frequency. By subtracting HASE frequency from total frequency the window for LASE was set at $\Delta F/F0 < 0.3$ (refer to Figure 2B, green-dashed lines). Total SCO amplitude was scored using *Average Peak Amplitude* with *Configure Peak Detection* settings: smooth width 1, fit width 3, slope threshold 0.01, and amplitude threshold dynamic 7. Changes in each well were normalized to their respective baseline recording and used to determine significant changes in frequency and amplitude for each therapeutic candidate. GraphPad Prism software (Version 8; San Diego, California) was used for statistical analysis and graphing. Where applicable, IC_{50} and EC_{50} values were determined using a nonlinear regression, 3-parameter logistic equation. For post hoc multiple comparison, separate 1-way ANOVA using a Tukey test was applied. Data are presented as the mean $\pm$ SEM.

ESA measured by microelectrode array. Microelectrode array technology permits simultaneous recording of field potential events, termed ESA and provides robust measures of network electrical activity (Biffi et al., 2013; Colombi et al., 2013; Massobrio et al., 2015). The technology is especially powerful in identifying the onset of functional deficits elicited by disease causing mutations (Cao et al., 2012b) and neurotoxicological responses to environmental chemicals (Frank et al., 2017). ESA patterns were measured from neuronal/glial coculture model described above plated on multiple electrode locations. Specifically, postnatal day 0/1 hippocampal neurons were plated onto either 12-well (64 electrodes/well) or 48-well (16 electrodes/well) Maestro system microelectrode array plates (Axion BioSystems, Atlanta, Georgia). ESA was recorded at 14 DIV to measure the acute effect of TETS and therapeutic candidates. Plates were transferred from the cell incubator to a prewarmed head-stage containing the recording amplifier. Signals were digitized at 25 kHz and filtered using a Butterworth bandpass filter with cutoff frequencies of 200 and 3000 Hz. After recording baseline electrical activity for 10 min, TETS or therapeutic candidates were introduced alone or in combination with MDZ, and ESA recorded for another 10 min. Axis software was used to detect spontaneous ESA events that exceeded a threshold of 8 times the electrical noise with the prespike (0.84 ms, 11 samples) and the postspike (2.16 ms, 27 samples) with 1 s interval. Data files containing event timestamps for each electrode in each well were analyzed using Axion Integrated Studios V_2.4.2, (Axion BioSystems) for spike frequency and burst characteristics. Burst detector settings were as follows, inter-spike interval threshold (maximum interspike interval 100 ms, minimum number of spikes 5), network bursts (maximum interspike interval 100 ms, minimum number of spikes 10, minimum number of participating electrodes 25%), mean firing rate estimation (detection window 10 s), synchrony parameters (window size 20 ms). NeuroExplorer (Version 4.133; Colorado Springs, Colorado) was used to draw raster plots. Matlab (Mathworks, Natick, Massachusetts) was used to export spike plot data and generate spike waveforms from the microelectrode array data. SCO and electrical activity after drug exposure were compared with baseline activity on a well-by-well analysis.

Whole-cell patch-clamp recordings on recombinantly expressed GABAA receptors. The human $GABA_A$ receptors α_1, α_2, β_3, and γ_{2L} and the rat β_2 cloned into pcDNA3.1 expression vectors were a generous gift from Dr Robert L. Macdonald, Vanderbilt University, TN. L929 cells, a murine fibroblast cell line obtained from ATCC (American Type Culture Collection, Manassas, Virginia) were cultured in Dulbecco's modified Eagle's medium (Lonza, Basel, Switzerland) supplemented with 10% FBS, 100 U/ml penicillin and 100 mg/ml streptomycin (Invitrogen, ThermoFisher, Grand Island, New York) and maintained in humidified 95% air and 5% CO_2 air at 37°C. Cells were transfected using FuGENE 6 (ThermoFisher) transfection reagent with an equal amount of each of the subunits in combination with pEGFP-C1. Two days posttransfection, cells were plated on glass coverslips and transfected cells were identified before recordings by their green fluorescence. Whole-cell voltage-clamp recordings were performed at room temperature with an EPC-10 HEKA amplifier. Cells were bathed in external Ringer solution consisting of 160 mM NaCl, 4.5 mM KCl, 1 mM $MgCl_2$, 2 mM $CaCl_2$, 10 mM HEPES, pH 7.4, and 308 mOsm. Recording electrodes were pulled from soda lime glass micro-hematocrit tubes (Kimble Chase, Rochester, New York) and fire-polished to resistances of 1.8–3 MΩ. Electrodes were filled with an internal solution consisting of 154 mM KCl, 2 mM $CaCl_2$, 1 mM $MgCl_2$, 10 mM HEPES, and 10 mM EGTA with pH 7.2 and 302 mOsm. Cells were voltage clamped at -80 mV and control currents were recorded under the application of EC_{10} GABA, using a gravity-fed fast perfusion system (VC38 system, ALA Scientific), for 5 s followed by a 40–50 s wash with external solution. GABA concentration-response relationships were determined by testing increasing concentrations of GABA and normalizing GABA currents to the peak response induced by a saturating concentration of GABA. Normalized currents were fitted using the Hill equation to determine the GABA EC_{10} values for the $\alpha_1\beta_2\gamma_{2L}$ (1 μM) and the $\alpha_2\beta_3\gamma_{2L}$ (2 μM) receptor. The EC_{10} was then used to evaluate the positive modulatory effects of ALLO, ELTAN, and MDZ. The increases in Cl^- current elicited in the presence of compounds were compared with the initial EC_{10} to determine the fold increase in current. Data fitting to the Hill equation to obtain EC_{50} values was performed using Origin 9.1 software (OriginLab Corporation). Individual data points are presented as mean $\pm$ SD from 4-8 independent recordings. EC_{50} values were calculated with 95% CIs using Origin (Version 9.1; Northampton, Massachusetts).

RESULTS

### Mouse Primary Hippocampal Neuron/Glia Cocultures as a Model System

Hippocampal neuronal/glial cocultures were fixed and immunostained at 14 DIV using antibodies that recognize either neuron- or glia-specific proteins (MAP2 and GFAP, respectively). Nuclei were stained with NucBlue. MAP2 staining revealed neuronal soma with extensive dendritic processes (Figure 1A, green channel). GFAP staining showed glia exhibiting different degrees of ramification (Figure 1A, red channel). Neurons typically grew over the glial layer, although in some areas the 2 cell types interdigitated (Figure 1A, overlay), suggesting spatially close associations of the cell types. Under these experimental conditions, the cultures consisted of neuron: glia cell ratios ranging from 1:1 to 1:2 based on the averaged immunostaining density of green: red channels. Distinct staining patterns for vGAT (Figure 1B, red channel) and vGLUT1 (Figure 1B, blue channel) were found, indicating the presence of inhibitory and excitatory neurons, respectively. Punctate staining of vGAT was found near neural soma and extending into proximal dendrites, and possibly axons of vGLUT-expressing neurons; the latter representing the predominant cell type (Figure 1B, see Overlay and
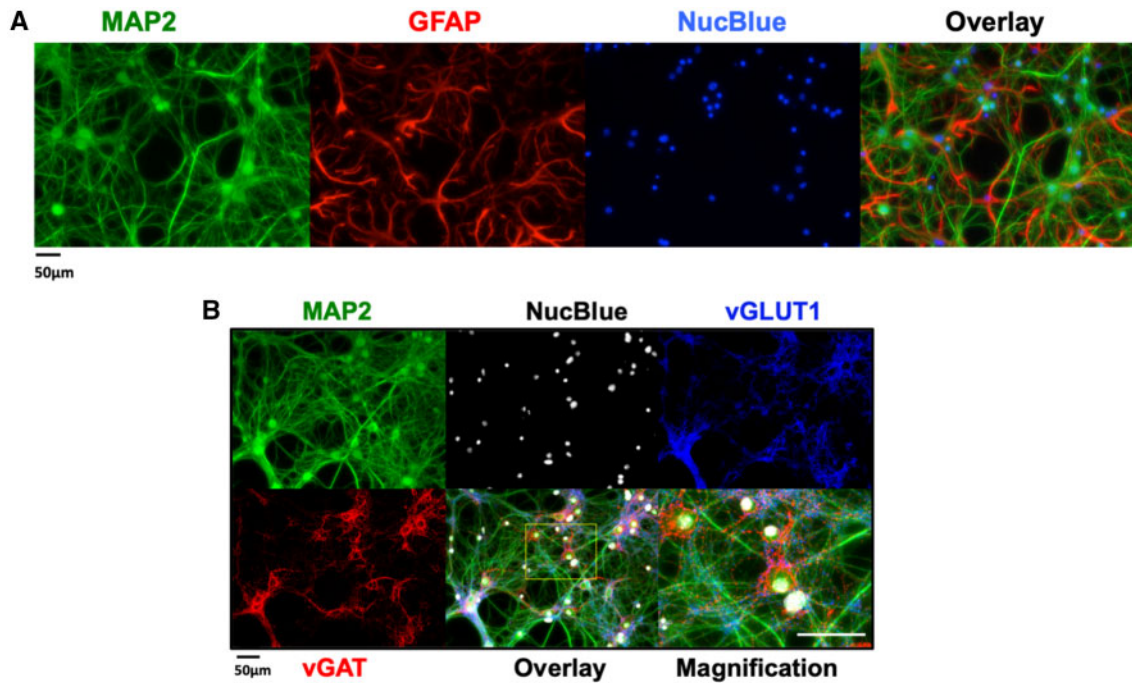
Figure 1. Mouse hippocampal neuron and glia co-culture at 14 days *in vitro* (DIV) express both glutamatergic and GABAergic neurons. A, Representative immunocyto-fluorescence images showing the neuronal/glial cultures at 14 DIV used to perform functional studies. Neuronal soma, axons and dendritic processes were stained with MAP2 and glia stained with GFAP. Nuclei were stained with NucBlue. Right-most panel is an overlay of all 3 stains. B, Representative immunocytofluorescence images showing the distribution of vesicular GABA transporters (vGAT) and vesicular glutamate transporters within MAP2 positive neurons. The overlay at higher resolution resolves the punctate pattern of the vGAT positive GABAergic neurons.
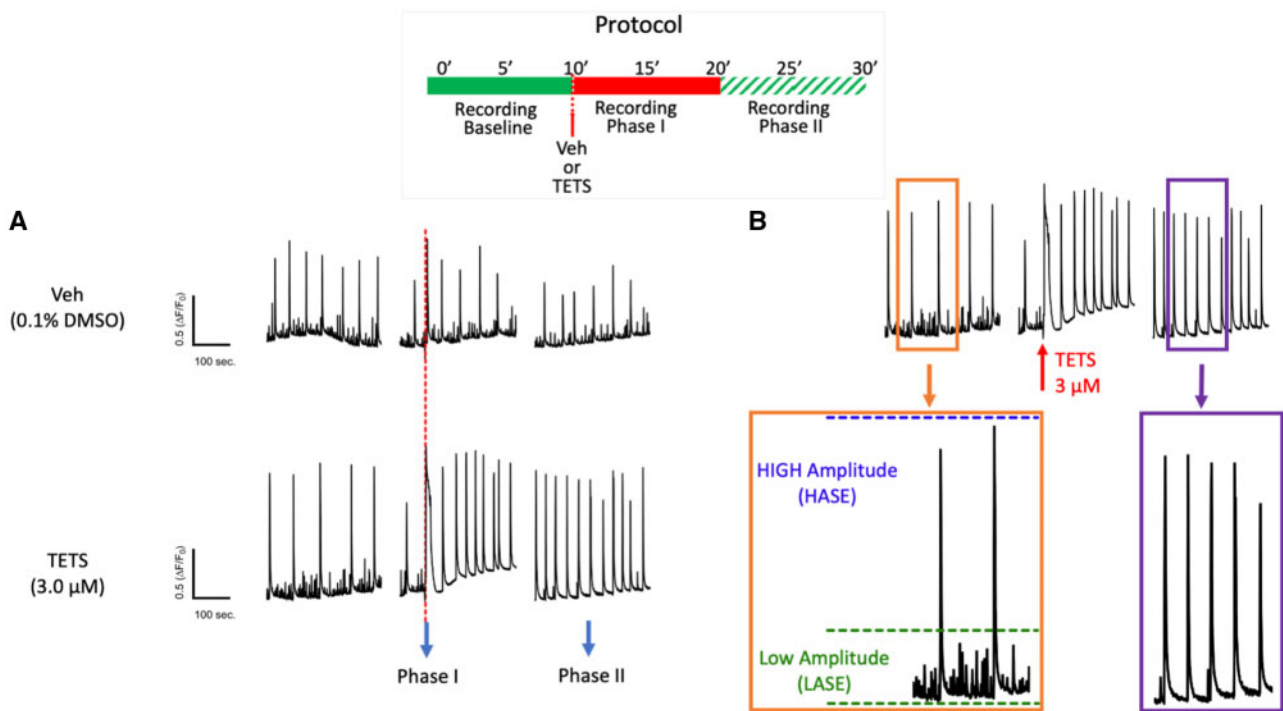
Figure 2. Tetramethylenedisulfotetramine (tetramine or TETS) triggers rapid overall changes in neuronal network synchronous Ca^{2+} oscillation (SCO) patterns by stabilizing high amplitude SCO events (HASE) and eliminating low amplitude SCO events (LASE). Graphic representation of the experimental protocol (inset). A, representative SCO traces before (Baseline) and after addition of TETS (3.0 μM) illustrate a rapid but transient rise in cytoplasmic Ca^{2+} (phase I response) and subsequent alterations in 2 distinct populations of SCO events: HASE and LASE (phase II response). Vehicle (0.01% DMSO) showed no significant influences on SCO during either Phase of recording. B, Magnified traces recorded during Baseline, phases I and II; Orange box: Baseline activity showing the green-dashed line is the cut-cutoff thresholds for binning LASE ($\Delta F/F0 \leq 0.3$) and the blue-dashed line is the binning cutoff for HASE. Purple box: typical phase II response after applying 3 μM TETS, which eliminates all LASE.
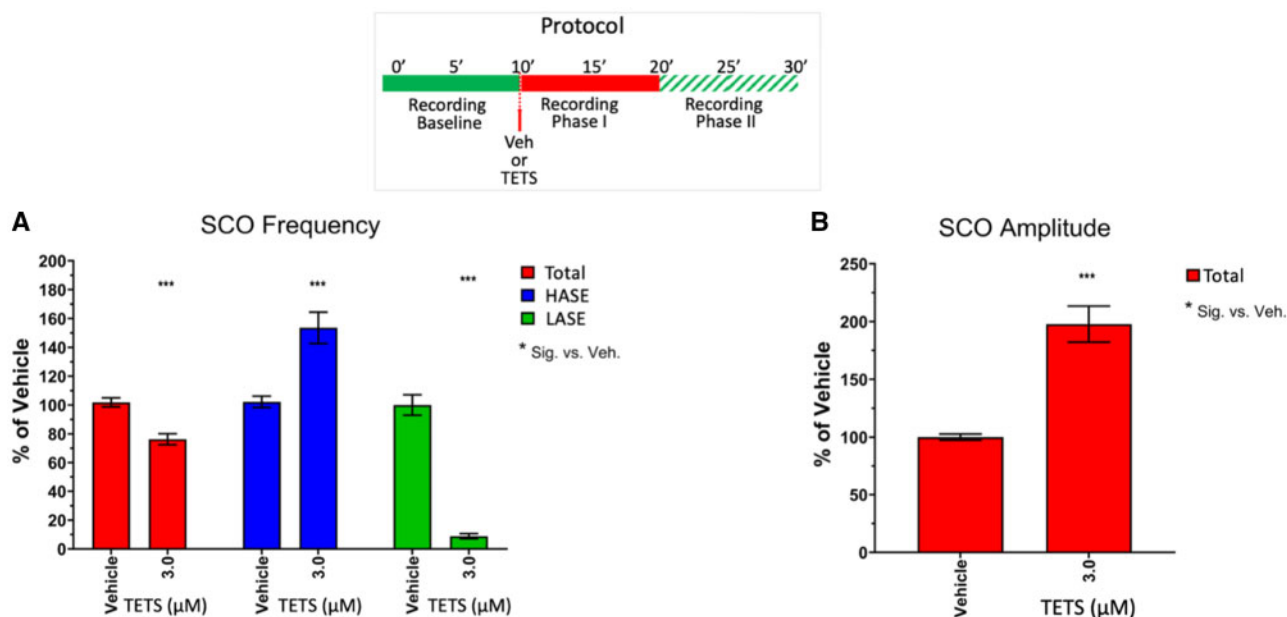
Figure 3. Tetramethylenedisulfotetramine (tetramine or TETS; 3 μM) decreases overall total SCO frequency and increases SCO amplitude by stabilizing high amplitude SCO events (HASE) and suppressing low amplitude SCO events (LASE). Upper panel shows the experimental protocol for recording baseline and phases I and II recordings postaddition of TETS (3.0 μM). A, Total SCO frequency (red bars), HASE (blue bars) and LASE (green bars) and (B) total amplitude are measured after addition of TETS and normalized to Vehicle control (0.01% DMSO). Total frequency and amplitude are measures of all events (HASE+LASE). All responses to TETS are normalized to respective vehicle controls and reported as mean ± SEM percent change ($n = 10$–15 wells measured on 3 independent culture days). ANOVA with Tukey post hoc correction $*p < .05$; $**p < .01$; $***p < .001$.

Magnification panels). The presence of both GABAergic and glutamatergic neurons is consistent with reports from primary cultures of cortex and hippocampus from rat or mouse (Björklund et al., 2010; Cao et al., 2017; Frank et al., 2017; Koga et al., 2010).

TETS Dysregulates 2 Types of SCOs

During recordings of baseline SCO activity, cultured hippocampal neurons exhibited 2 distinct patterns of SCOs at 14–16 DIV: Low- and High-amplitude SCO events, which we termed LASE and HASE, respectively (Figs. 2A and 2B). Both LASE and HASE activities were rapidly eliminated by addition of TTX to block axonal voltage-dependent Na$^+$ channels (Supplementary Figs. 2A and 2B), indicating that both LASE and HASE were dependent on Na$^+$ channel activity and overall ESA of neuronal networks as described by Shafer and coworkers (McConnell et al., 2012). Therefore, the amplitude and frequency of LASE and HASE were quantified together (pooled event data we termed total amplitude or total frequency) or analyzed separately. The sequence of obtaining data from each experimental protocol is summarized at the top of each figure. For instance, Figure 2A shows simultaneous recordings of baseline SCO activities from individual culture wells for 10 min at which time either vehicle (Veh) or TETS (3.0 μM) was added to separate wells. Recordings continued for an additional 20 min. A characteristic sharp rise in baseline Ca^{2+} was seen immediately after TETS addition as previously reported (Cao et al., 2012a) and termed "Phase I" (Figure 2A). The current study focused on quantifying subsequent changes in SCO patterns (termed "Phase II") measured during the last 5 min of each recording to calculate IC$_{50}$, EC$_{50}$ values, or quantitatively compare drug responses at specified concentrations as described in Materials and Methods section.

Vehicle (0.1% DMSO) had no significant effect on SCO properties during Phases I or II and was used to normalize responses to TETS exposure (Figs. 2A and 3). Under control recording conditions, the frequency of LASE was significantly higher than HASE (control frequencies: Mean ± SEM for LASE = 4.03 + 0.19, 95% CI = 3.64–4.41 min^{-1}; Mean ± SEM for HASE 2.89 ± 0.124, 95% CI = 2.65–3.14 min^{-1}). TETS (3.0 μM) significantly reduced overall mean network frequency to 76.3% ± 3.8% of the frequency measured during the respective time period in the Vehicle controls (Figure 3A, red bars) and increased total amplitude 1.98 ± 0.16-fold (Figure 3B). Closer inspection of SCO patterns revealed that TETS (3.0 μM) eliminated LASE while HASE frequency was significantly increased compared with control at this concentration (Figure 3A, compare green and blue bars). Specifically, TETS (3.0 μM) increased the amplitude of HASE by nearly 2-fold (197% ± 21% Mean ± SEM; 95% CI 154.2–239.0; $p < .001$).

SCO activity reflects the balance of excitatory/inhibitory receptor inputs placed on individual neurons and the networks they form in the hippocampal model used here (Figure 1) and were previously shown to be highly sensitive to modulation by glutamatergic and GABAergic pharmacology (Cao et al., 2015, 2017; Smedler and Uhlén, 2014). To this point, PERAMP, a selective AMPA receptor antagonist approved for treatment of partial seizures and generalized tonic-clonic seizures, inhibited TETS-triggered SCO activity, concomitantly reducing both total SCO frequency (IC$_{50}$ = 149 nM; 95% CI: 68.4–309.6 nM) and total SCO amplitude (IC$_{50}$ = 135 nM; 95% CI: 7.6–727 nM; Figs. 4A and 4B, red bars). PERAMP depressed TETS-triggered HASE activity in a concentration-dependent manner, but failed to recover the activity of LASE across the entire concentration range tested (Figure 4A, compare blue and green bars), a range that completely suppressed all neuronal network activity at 3 μM (Figs. 4A and 4B, red bars).

The positive allosteric GABA$_A$R modulator MDZ, an exemplary benzodiazepine and the current standard of care for threat agents such as TETS and organophosphates (Jett and Spriggs,
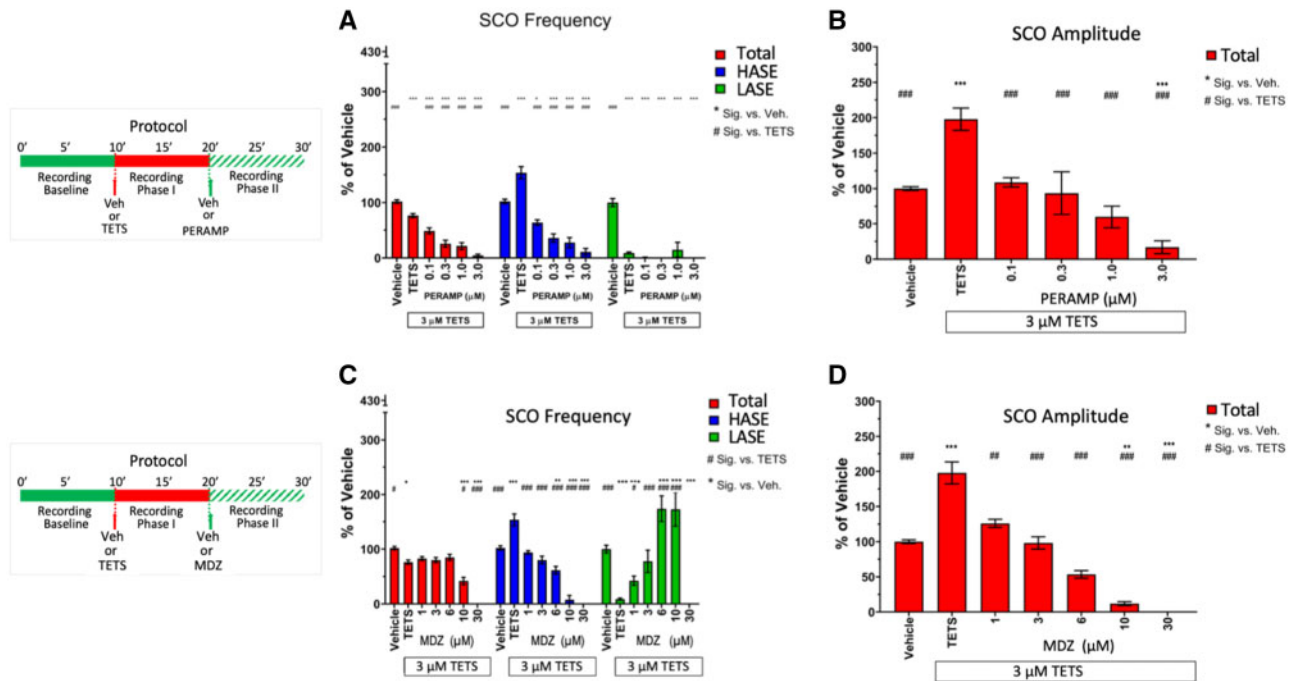
Figure 4. Perampanel (PERAMP) and midazolam (MDZ) mitigate tetramethylenedisulfotetramine (tetramine or TETS) -triggered synchronous Ca^{2+} oscillation patterns. Upper panels in (A) and (B) show the experimental protocol for recording baseline and phases I and II recordings postaddition of TETS (3.0 μM) and subsequent addition of either PERAMP (0.1–3.0 μM) or MDZ (1–30 μM), respectively. Only phase II responses are analyzed in this study. A, PERAMP and (B) MDZ total amplitude (red bars), high amplitude SCO events (blue bars) and low amplitude SCO events (green bars) are normalize to Vehicle control (0.01% DMSO) and statistically compared with Vehicle (*) or TETS (#) using ANOVA with Tukey post hoc correction. Mean ± SEM ($n = 8$–15 wells measured on 3 independent culture days). *,#$p < .05$; **,##$p < .01$; ***,###$p < .001$. Summary statistics are reported in Table 1.

2018), elicited a distinct pharmacological profile toward TETS-triggered SCO patterns. Using the same protocol described earlier, MDZ significantly reversed TETS-triggered total SCO amplitude between 1 and 10 μM without influencing total SCO frequency; only at >10 μM did MDZ suppress network activity below those measured in Vehicle control (Figs. 4C and 4D, red bars). Unlike PERAMP, MDZ reciprocally reversed the influences of TETS on HASE and LASE within its pharmacologically active range of 1–30 μM (Figure 4a, blue and green bars, respectively). Table 1 summarizes comparisons between PARAMP and MDZ across the range of concentrations tested.

SAR Among 5 NAS and Cortisol Toward Normalizing TETS-Triggered SCO Patterns

Endogenous NASs, exemplified by ALLO (3α-hydroxy-5α-pregnan-20-one), increase the affinity of synaptic and extrasynaptic GABA$_A$R to GABA at low concentrations by acting as PAMs and thus amplify neuronal network inhibition. At higher concentrations, NAS also directly activate chloride current through their interactions with GABA$_A$R in the absence of GABA (ie, behave as direct activators) to further promote network inhibition. ALLO has been proposed as a novel therapeutic intervention to mitigate TETS-triggered seizures (Bruun et al., 2015; Cao et al., 2012a,b; Pessah et al., 2016), however its potency and efficacy has not been directly compared with chemically related NAS using SCO patterns in neuronal networks as an outcome measure of potential therapeutic benefit under identical assay conditions. NAS are highly lipophilic molecules with limited solubility in aqueous buffers. For these studies NAS concentrations were tested to a maximum of 3 μM to minimize potential confounding influences of precipitation. ALLO and other NAS were added to culture wells once TETS-triggered effects (relative to

corresponding activity observed in the Vehicle control during the same time period) were fully manifest. Figure 5 illustrated that ALLO (0.1–1.0 μM) had no significant influence on the TETS-triggered reduction of total SCO frequency until a concentration of 3 μM was applied, a concentration that normalized total frequency to that measured in Vehicle control (Figure 5A, red bars). In contrast, ALLO suppressed TETS-triggered elevation of total SCO amplitude across the entire concentration range tested (Figure 5B, red bars), an effect attributed to selective suppression of HASE frequency to control levels (Figure 5a, blue bars). Only at the highest concentration tested (3 μM) did ALLO significantly increase LASE frequency to a level approximately 214% of Vehicle control (Figure 5B, green bars), likely the result of direct GABA$_A$R activation (Nik et al., 2017; Reddy and Estes, 2016). In support of this interpretation, GABA itself (0.1–3.0 μM) was found to decrease HASE and increase LASE frequency in a concentration dependent manner (Supplementary Figure 6A) with only modest suppression of total SCO amplitude (Supplementary Figure 6B). Only at 10 μM GABA were all network SCO activities suppressed.

ELTAN (3α-hydroxy-5β-pregnan-20-one), the positional isomer of ALLO (Supplementary Figure 1), had no significant influence on either TETS-triggered SCO total frequency or amplitude below 1 μM (Figs. 5C and 5D, red bars). Interestingly, ELTAN (0.1 and 0.3 μM) significantly augmented the frequency of TETS-triggered HASE, whereas 1 μM reduced and 3 μM eliminated all HASE activity (Figure 5C, blue bars). The bell-shaped influences of ELTAN on HASE occurred with a concentration dependent increase in LASE reaching significance at >1 μM and reaching 302% of vehicle at 3 μM (Figure 5C, green bars).

Using single-cell voltage-clamp, we further investigated whether differences in the activity of ALLO and ELTAN on TETS-

Table 1. SCO Amplitude and Frequency Response to AMPAR Antagonist PERAMP or GABAAR PAM MDZ Added to Mouse Hippocampal Neuronal Cultures Exposed to 3 µM TETS at DIV 14–16

Treatment	Mean (% of Vehicle)	SEM	95% CI		Vs Vehicle p	Vs TETS p
			Upper	Lower		
SCO frequency: PERAMP						
Vehicle	100.00	2.57	105.19	94.79		.0021
TETS	76.25	3.82	83.98	68.52	.0021	
0.1 µM PERAMP + TETS	48.68	5.46	60.39	36.97	<.0001	.0177
0.3 µM PERAMP + TETS	25.63	6.06	38.62	12.63	<.0001	<.0001
1.0 µM PERAMP + TETS	21.40	6.07	34.43	8.37	<.0001	<.0001
3.0 µM PERAMP + TETS	4.43	2.46	9.70	0.00	<.0001	<.0001
SCO amplitude: PERAMP						
Vehicle	100.00	2.69	105.36	94.64		<.0001
TETS	197.79	15.63	228.94	166.64	<.0001	
0.1 µM PERAMP + TETS	108.75	6.57	122.85	94.66	.7398	.0007
0.3 µM PERAMP + TETS	93.48	30.20	158.25	28.70	.8044	<.0001
1.0 µM PERAMP + TETS	59.75	15.61	93.23	26.28	.1269	<.0001
3.0 µM PERAMP + TETS	16.87	9.05	36.27	0.00	.0017	<.0001
SCO frequency: MDZ						
Vehicle	100.00	2.57	105.19	94.79		.0021
TETS	76.25	3.82	83.98	68.52	.0021	
1.0 µM MDZ + TETS	82.92	3.44	90.69	75.15	.1963	.6144
3.0 µM MDZ + TETS	80.08	4.68	90.68	69.49	.0985	.7721
6.0 µM MDZ + TETS	84.86	5.55	97.42	72.31	.1971	.5153
10.0 µM MDZ + TETS	41.86	6.69	57.68	26.03	<.0001	.0179
SCO amplitude: MDZ						
Vehicle	100.00	2.69	105.36	94.64		<.0001
TETS	197.79	15.63	228.94	166.64	<.0001	
1.0 µM MDZ + TETS	125.99	5.81	139.13	112.86	.407	.0221
3.0 µM MDZ + TETS	98.13	8.74	117.90	78.36	.9523	.0015
6.0 µM MDZ + TETS	53.46	5.38	65.63	41.29	.1378	<.0001
10.0 µM MDZ + TETS	11.88	2.71	18.13	5.62	.0074	<.0001
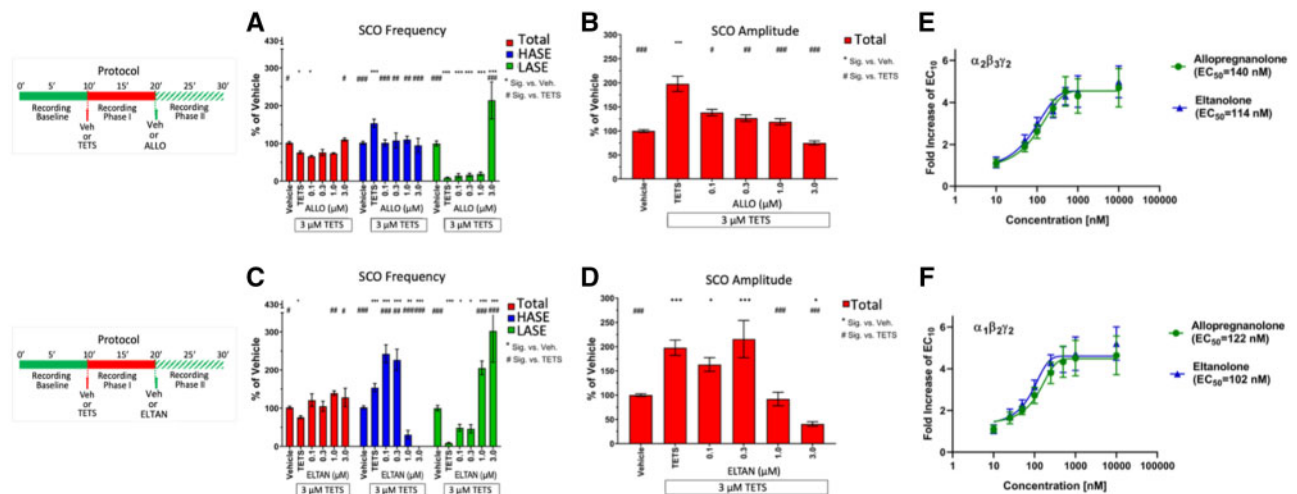
Figure 5. Allopregnanolone (ALLO) and eltanolone (ELTAN) differentially mitigate tetramethylenedisulfotetramine (TETS)-triggered SCO patterns. Upper panels in (A–D) show the experimental protocol for recording SCO during baseline and phases I and II postaddition of TETS (3.0 µM) and subsequent addition of either 0.1–3.0 µM ALLO or 0.1–3.0 µM ELTAN, respectively. Only phase II responses are analyzed in this study. A–D, Total amplitude (red bars), high amplitude SCO events (blue bars) and low amplitude SCO events (green bars) are normalize to Vehicle control (0.1% DMSO) and statistically compared with Vehicle (*) or TETS (#) using ANOVA with Tukey post hoc correction. Mean ± SEM ($n = 14$–15 wells measured on 3 independent culture days). *,#$p < .05$; **,##$p < .01$; ***,###$p < .001$. Summary statistics are reported in Table 2. E, Concentration-response curves for ALLO and ELTAN induced potentiation of peak inward Cl⁻ current responses of $\alpha_1\beta_2\gamma_2$ gamma-aminobutyric acid (GABAA) receptors to 1 µM GABA (EC_{10} value) in patch-clamp recordings. EC_{50} values for ALLO and ELTAN are 122 nM (95% CI: 105–139 nM) and 102 nM (95% CI: 76–128 nM) when concentration response curves are fitted with a Hill coefficient of 1.0. F, Concentration-response curves for ALLO and ELTAN induced potentiation of peak inward Cl⁻ current responses of $\alpha_2\beta_3\gamma_2$ GABAA receptors to 2 µM GABA (EC_{10} value). EC_{50} values for allopregnanolone and eltanolone are 140 nM (95% CI: 121–159 nM) and 114 nM (95% CI: 97–131 nM). Each data point is the mean ± SD of measurements of 4–8 cells.
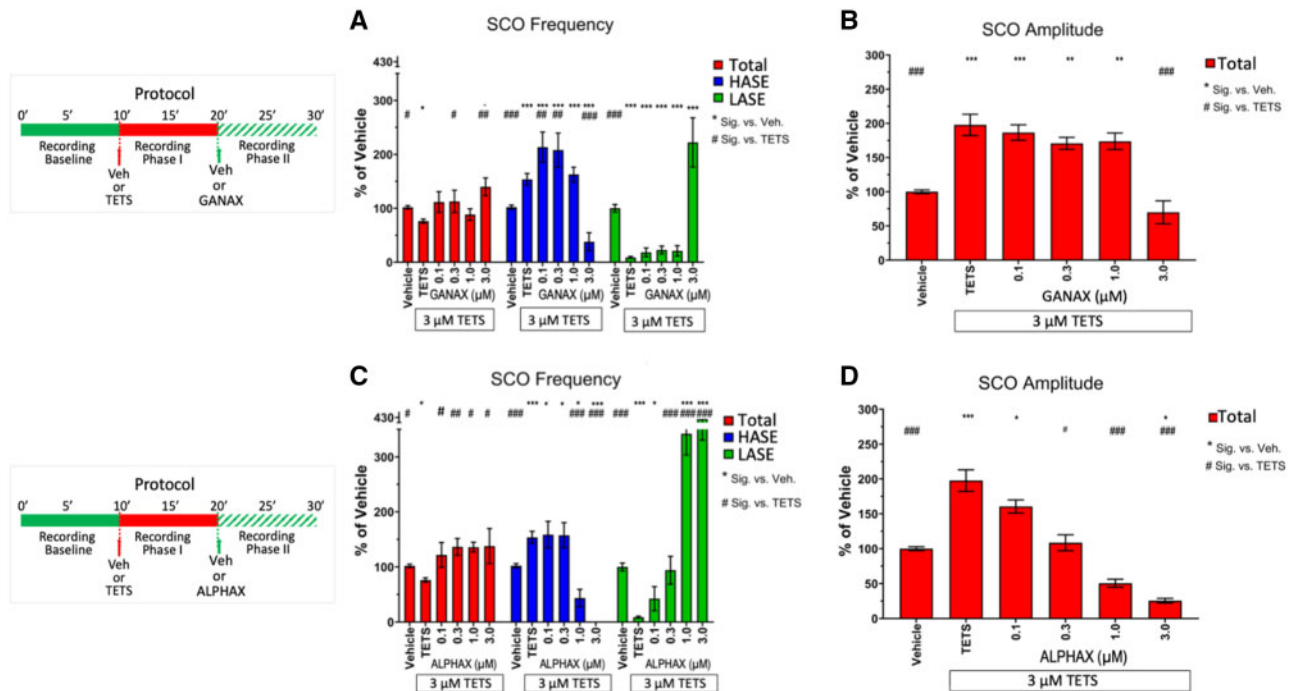
Figure 6. Ganaxolone (GANAX) and alphaxolone (ALPHAX) differentially mitigate tetramethylenedisulfotetramine (TETS)-triggered SCO patterns. Upper panels in (A–D) show the experimental protocol for recording SCO during baseline and phases I and II postaddition of TETS (3.0 μM) and subsequent addition of either 0.1–3.0 μM GANAX or 0.1–3.0 μM ALPHAX, respectively. Only phase II responses were analyzed in this study. A–D, Total amplitude (red bars), high amplitude SCO events (blue bars) and low amplitude SCO events (green bars) are normalize to Vehicle control (0.01% DMSO) and statistically compared with Vehicle (*) or TETS (#) using ANOVA with Tukey post hoc correction. Mean ± SEM (n = 9–15 wells measured on 3 independent culture days). *,#$p < .05$; **,##$p < .01$; ***,###$p < .001$. Summary statistics are reported in Table 2.

modified neuronal network activity was at least in part due to differential PAM activity toward GABA$_A$R of defined subunit composition. The 2 receptor combinations in Figures 5E and 5F were chosen because $\alpha_1\beta_2\gamma_2$ receptors constitute the most widely expressed GABA$_A$ receptor in the CNS (Rudolph and Knoflach, 2011), whereas $\alpha_2\beta_3\gamma_2$ receptors are the most TETS sensitive receptors (Pressly et al., 2018). When tested in the presence of a GABA concentration sufficient to elicit 10% of maximum Cl$^-$current amplitude ALLO and ELTAN exhibited indistinguishable potency and efficacy toward $\alpha_2\beta_3\gamma_2$ and $\alpha_1\beta_2\gamma_2$ channels demonstrating that their differential effects on SCO patterns do not seem to be due to differential effects on these 2 major synaptic GABA$_A$ receptors.

GANAX (3α,5α)-3-hydroxy-3-methyl-pregnan-20-one) produced similar patterns to those described for ELTAN once added to TETS-modified neuronal networks, with the following differences. Although total SCO frequency increased with ELTAN >0.3 μM, it did so without significant reductions in total SCO amplitude until the highest concentration (3 μM) was reached (Figs. 6A and 6B, red bars). Like ELTAN, GANAX altered HASE in a bell-shaped manner, significantly augmenting the TETS effect between 0.1 and 0.3 μM, with higher concentrations eliciting a sharp reduction. In contrast to ELTAN, GANAX did not completely eliminate HASE and only increased the frequency of LASE at the highest concentration tested to 222% of vehicle control (Figure 6A, green bars).

ALPHAX ((3α,5α)-3-hydroxypregnane-11,20-dione) was the most potent NAS tested, reversing the TETS pattern for total SCO frequency and amplitude in a concentration dependent manner across the entire concentration range tested (Figs. 6C and 6D, red bars). Unlike ELTAN and GANAX, ALPHAX did not augment TETS-triggered HASE at any concentration tested,

while dramatically reducing HASE and increasing LASE frequency at > 1 μM (Figure 6C, compare blue and green bars).

Unlike any of the biosynthesized NAS reported above, the synthetic XJ-42 ((3α,5α,20E)-3-hydroxy-13,24-cyclo-18-norcholan-20-ene-21-carbonitrile) at 0.1 μM further augmented TETS-triggered increase of total SCO frequency and SCO amplitude before inhibiting these parameters at higher concentrations (Supplementary Figs. 3A and 3B, red bars). At concentrations > 1 μM, XJ-42 reduced HASE and increased LASE in a reciprocal manner (Supplementary Figure 3A, blue and green bars). Finally, cortisol <1 μM introduced to the cells subsequent to TETS had no measurable influence on any TETS-triggered SCO pattern, whereas >1 μM only exacerbated HASE frequency (Supplementary Figure 4).

Table 2 summarizes results from ANOVA analysis comparing the TETS-induced pattern versus the control period (Vehicle) and then the relative effect of each NAS added on the TETS-triggered patterns in total SCO frequency and amplitude. At the lowest concentration tested (0.1 μM), ELTAN, GANAX, ALPHAX, and XJ-42 increased TETS-triggered reductions in SCO total frequency by 10–20% ($p < .05$), levels not different from Vehicle control, whereas 0.1 μM ALLO had no influence on TETS-triggered total SCO frequency (Table 2, first panel). At this concentration, ALLO normalized whereas XJ-42 increased mean SCO total amplitude nearly 3-fold greater than Vehicle control (Table 2, first panel), primarily driven by the increased frequency of HASE (Supplementary Figure 3a, blue bar). Of the NAS tested, only ALLO mitigated TETS-triggered SCO patterns in the neuronal networks across its entire concentration range toward patterns measured with Vehicle control, primarily by normalizing HASE and ultimately stabilizing LASE, without suppression of total SCO frequency or amplitude below those measured in

Table 2. SCO Frequency and Amplitude Response to 5 NAS Added to Mouse Hippocampal Neuronal Cultures Are Exposed to 3 μM TETS at DIV 14–16

Treatment	Mean (% of Vehicle)	SEM	95% CI		Vs Vehicle p	Vs TETS p
			Upper	Lower		
SCO frequency: 0.1 μM NAS						
Vehicle	100.00	2.57	105.19	94.79		.0021
TETS	76.25	3.82	83.98	68.52	.0021	
ALLO + TETS	66.28	2.27	71.16	61.41	.002	.3901
ELTAN + TETS	120.92	16.51	156.34	85.50	.0968	.0001
GANAX + TETS	111.57	19.11	152.85	70.29	.4085	.0031
ALPHAX + TETS	121.73	22.44	172.49	70.97	.1395	.0008
XJ-42 + TETS	111.97	13.25	140.38	83.56	.3774	.0021
SCO frequency: 0.3 μM NAS						
Vehicle	100.00	2.57	105.19	94.79		.0021
TETS	76.25	3.82	83.98	68.52	.0021	
ALLO + TETS	76.24	8.23	94.02	58.46	.0289	.9991
ELTAN + TETS	105.01	12.98	132.85	77.17	.7799	.0126
GANAX + TETS	112.75	20.69	157.45	68.06	.3499	.0021
ALPHAX + TETS	136.35	15.15	170.62	102.08	.0099	<.0001
XJ-42 + TETS	119.83	18.21	158.87	80.78	.1143	.0002
SCO frequency: 1.0 μM NAS						
Vehicle	100.00	2.57	105.19	94.79		.0021
TETS	76.25	3.82	83.98	68.52	.0021	
ALLO + TETS	73.97	1.64	77.48	70.46	.0147	.8427
ELTAN + TETS	139.38	5.98	152.20	126.55	.001	<.0001
GANAX + TETS	88.32	10.64	111.30	65.34	.2478	.3062
ALPHAX + TETS	135.82	8.79	155.70	115.93	.0111	<.0001
XJ-42 + TETS	121.49	15.25	154.19	88.79	.0846	<.0001
SCO frequency: 3.0 μM NAS						
Vehicle	100.00	2.57	105.19	94.79		.0021
TETS	76.25	3.82	83.98	68.52	.0021	
ALLO + TETS	110.51	3.82	118.71	102.31	.4456	.003
ELTAN + TETS	127.98	24.18	179.85	76.11	.022	<.0001
GANAX + TETS	139.84	16.47	175.42	104.26	.0012	<.0001
ALPHAX + TETS	137.78	31.82	211.15	64.41	.0101	<.0001
XJ-42 + TETS	100.14	4.20	109.21	91.06	.885	.0431
SCO Amplitude: 0.1 μM NAS						
Vehicle	100.00	2.69	105.36	94.64		<.0001
TETS	197.79	15.63	228.94	166.64	<.0001	
ALLO + TETS	138.30	6.47	152.18	124.43	.1539	.0267
ELTAN + TETS	157.53	11.29	182.14	132.92	.0438	.1576
GANAX + TETS	186.51	11.37	211.08	161.95	.0018	.6827
ALPHAX + TETS	160.48	9.44	181.84	139.12	.0585	.2424
XJ-42 + TETS	277.81	62.50	411.85	143.76	<.0001	.0029
SCO amplitude: 0.3 μM NAS						
Vehicle	100.00	2.69	105.36	94.64		<.0001
TETS	197.79	15.63	228.94	166.64	<.0001	
ALLO + TETS	126.57	6.89	141.45	111.69	.3254	.0085
ELTAN + TETS	215.63	38.16	298.07	133.20	<.0001	.5085
GANAX + TETS	170.72	8.77	189.82	151.63	.0113	.3309
ALPHAX + TETS	108.57	11.42	134.40	82.74	.7837	.0043
XJ-42 + TETS	228.05	42.19	318.54	137.56	<.0001	.2485
SCO amplitude: 1.0 μM NAS						
Vehicle	100.00	2.69	105.36	94.64		<.0001
TETS	197.79	15.63	228.94	166.64	<.0001	
ALLO + TETS	118.96	6.47	132.84	105.09	.4699	.0027
ELTAN + TETS	91.87	14.00	121.89	61.85	.7567	<.0001
GANAX + TETS	173.76	12.05	199.79	147.72	.0065	.373
ALPHAX + TETS	50.60	5.72	63.54	37.66	.1138	<.0001
XJ-42 + TETS	211.47	50.11	318.93	104.00	<.0001	.6019
SCO amplitude: 3.0 μM NAS						
R Vehicle	100.00	2.69	105.36	94.64		<.0001
TETS	197.79	15.63	228.94	166.64	<.0001	
ALLO + TETS	75.11	4.37	84.64	65.59	.3718	<.0001
ELTAN + TETS	40.48	4.68	50.53	30.44	.0236	<.0001
GANAX + TETS	69.97	16.81	106.28	33.66	.2662	<.0001
ALPHAX + TETS	25.59	3.30	33.06	18.12	.0173	<.0001
XJ-42 + TETS	59.17	4.96	69.89	48.45	.1308	<.0001
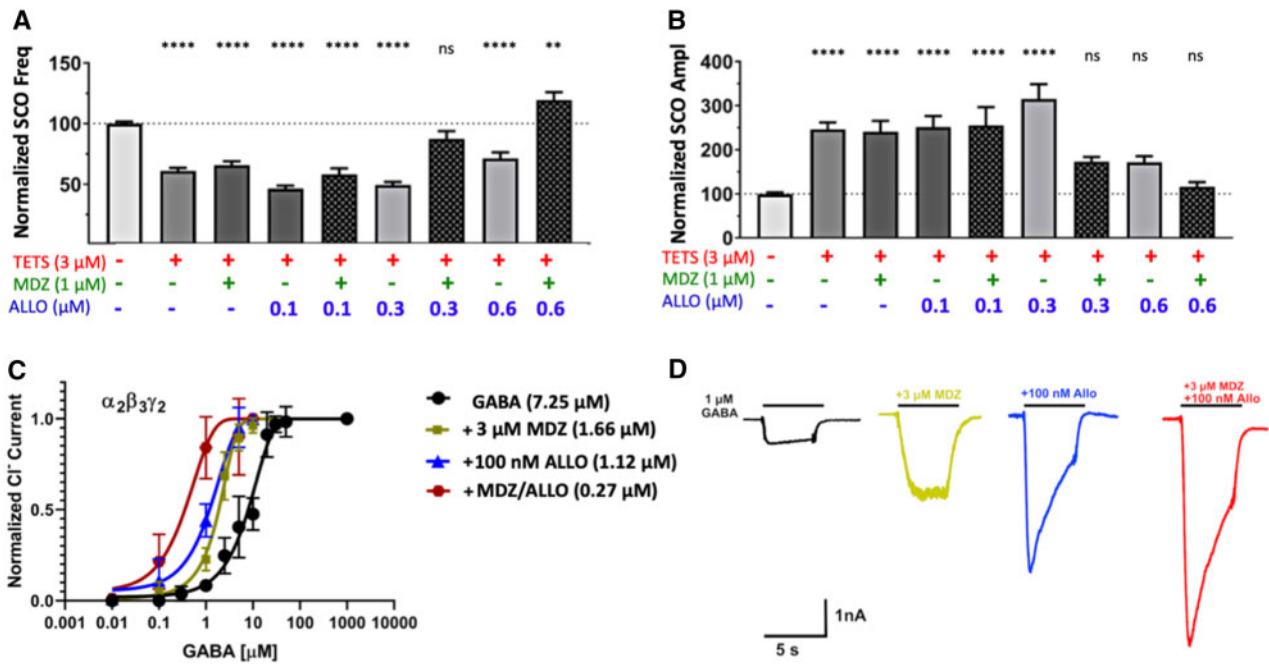
Figure 7. Midazolam (MDZ) in combination with allopregnanolone (ALLO) mitigates TETS-triggered SCO patterns at concentrations that are individually less effective and their combination is more potent as positive allosteric modulator. A and B, MDZ (1 μM) or ALLO (0.1-0.3 μM) applied individually do not significantly reverse tetramethylenedisulfotetramine (TETS)-triggered Ca^{2+} oscillation (SCO) dysregulation. MDZ (1 μM) in combination with ≥ 0.3 μM ALLO restored SCO to (frequency and amplitude), or above (frequency) respective measures in Vehicle control. One-way ANOVA with additional correction (Tukey) for post hoc multiple comparison was applied to determine the statistical differences. Each data point represents mean ± SEM of data from 10–15 wells. *$p < .05$; **$p < .01$; ***$p < .001$, and ****$p < .0001$. C, Effect of MDZ (3 μM), ALLO (100 nM) or of the combination of MDZ and ALLO on the gamma-aminobutyric acid (GABA) concentration response curve of $\alpha_2\beta_3\gamma_2$ GABA$_A$ receptors. GABA: EC$_{50}$ 7.25 μM (95% CI: 6.39–8.11 μM; $n_H = 1.66$); GABA + 3 μM MDZ: EC$_{50}$ 1.66 μM (95% CI: 1.57–1.74 μM; $n_H = 1.87$); GABA + 100 nM ALLO: EC$_{50}$ 1.12 μM (95% CI: 1.05–1.20 μM; $n_H = 1.30$); GABA + 3 mM MDZ + 100 nM ALLO: EC$_{50}$ 0.27 μM (95% CI: 0.12–0.42 μM; $n_H = 1.21$). D, Representative currents elicited by 1 μM of GABA in the absence and the presence of MDZ (3 μM), ALLO (100 nM) or of the combination of MDZ and ALLO are shown below the data plot. Each data point is the mean ± SD of measurements of 4–8 cells.

Vehicle control at 3 μM, the highest concentration tested (Figs. 5A and 5B; Table 2). In contrast, ELTAN (0.1–0.3 μM) and XJ-42 (0.1–1.0 μM) failed to decrease total SCO amplitude while significantly increasing HASE frequency above that of TETS alone (Figs. 5C and 5D, Supplementary Figs. 3A and 3B, and Table 2), a pattern also seen with 0.1–1.0 μM GANAX (Figs. 6A and 6B and Table 2). At the highest concentration tested ALLO, GANAX, and XJ-42 significantly stabilized LASE without significantly lowering mean total SCO amplitude below Vehicle control (Table 2).

### Efficacy of ALLO + MDZ on TETS-Triggered SCO Patterns and Cl⁻ Current

Our previous study on TETS (Cao et al., 2012a) indicated that a combination of ALLO and diazepam at low concentrations, which when used individually were inactive, was highly effective at reversing TETS-triggered SCO dysregulation. Considering that MDZ was recently approved as the new standard of care for treating threat-agent induced seizures (Jett and Spriggs, 2018), we asked the question of whether ALLO + MDZ added at concentrations below those needed individually were capable of mitigating TETS-triggered SCO network patterns. ALLO (as high as 0.6 μM) or MDZ (1 μM) added singly failed to significantly mitigate TETS-triggered reductions of total SCO frequency (Figure 7A), nor fully restored total SCO amplitude to the Vehicle control level (Figure 7). In contrast, combinations of 1 μM MDZ plus 0.3 or 0.6 μM ALLO restored both total SCO frequency and amplitude to levels not significantly different from Vehicle control (Figs. 7A and 7B). The influence of combinations of ALLO (0.1–1.0 μM) and MDZ (0.1–3.0 μM) on HASE and LASE frequency

as well as total amplitude are summarized in Supplementary Figure 5. From these concentration-effect relationships it is interesting to point out that ALLO (0.6 μM) in combination with the concentrations of MDZ tested (0.1 or 0.3 μM) is sufficient to normalize LASE and HASE patterns to those measured in corresponding Vehicle control, without suppressing overall neuronal network activity, ie, total SCO frequency and amplitude (Figs. 8E–G and Supplementary Figure 5, red bars).

Using the most TETS-sensitive $\alpha_2\beta_3\gamma_2$ receptor we further tested combinations of ALLO and MDZ and observed that the combination of 0.1 μM ALLO and 3 μM MDZ dramatically left-shifted the concentration-dependent activation of GABA-induced Cl⁻ current by 30-fold (Figs. 7C and 7D).

ALLO + MDZ at Low Concentrations Effectively Mitigate TETS-Triggered ESA

Spontaneous ESA across neuronal networks was measured using a microelectrode array approach described in the Materials and Methods (Figs. 8A–C). ESA patterns are composed of individual biphasic events that likely manifest by excitatory synaptic potentials (Figure 8B) and show spatial connectivity across the neuronal networks (Figure 8C). The frequency and patterns of ESA were recorded across the neuronal network to analyze for spike and burst frequency, burst duration and synchronicity. Baseline ESA was recorded for each well for 10 min, and then either vehicle (0.1% DMSO), 1 μM TETS, 0.1 μM ALLO, 0.1 μM MDZ, or the combination of 0.1 μM ALLO plus 0.1 μM MDZ were added to the separate wells. Network electrical activity was monitored for the next 10 min. Spike and burst analysis revealed that while
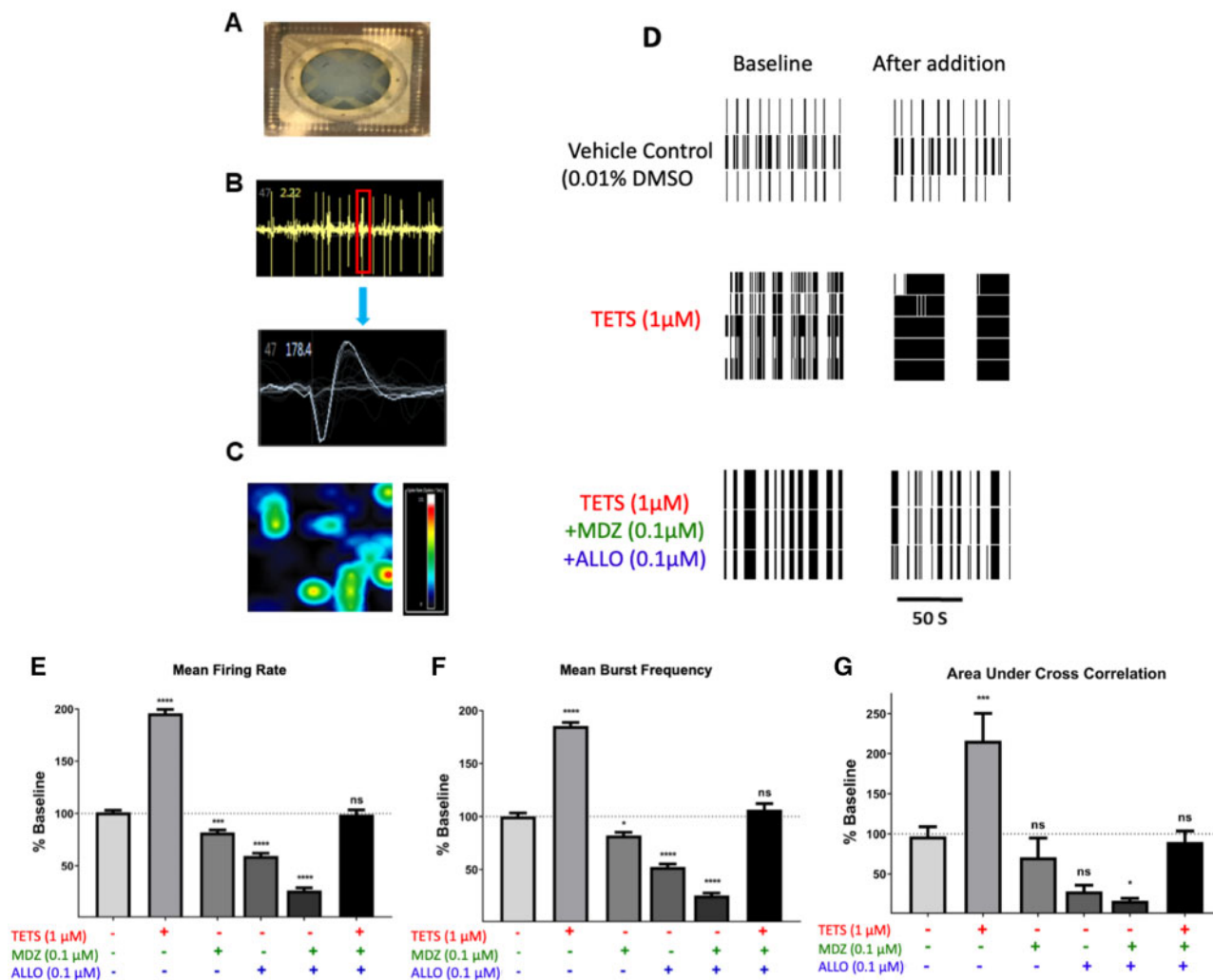
Figure 8. Abnormal network electrical spike activity (ESA) triggered by tetramethylenedisulfotetramine (TETS) is mitigated by the combination of midazolam (MDZ) and allopregnanolone (ALLO). A, ESA recordings were performed on 12 well microelectrode array plates consisting of 64 electrodes/well. B, Example of waveforms counted in ESA data capture using Axis software with the threshold set at 8 times the noise (faint gray trace in lower panel). C, Microelectrode array heat map shows the spatial distribution of ESA. D, Representative raster plots showing ESA activities before (Baseline) and after addition of TETS (1.0 μM) or TETS with the combination of MDZ (0.1 μM) and ALLO (0.1 μM). Summary data showing the influence of TETS, MDZ, and ALLO, singly or in combination, on Mean firing rate (E), mean burst frequency (F), and area under cross correlation—a measure of neuronal network synchronicity (G). ESA measures after TETS + drug additions are to their respective baseline periods before addition and statistically compared using ANOVA with Tukey post hoc correction. Mean ± SEM ($n = 5$–18 wells measured on 2–3 independent culture days). $^{*}p < .05$; $^{**}p < .01$; $^{***}p < .001$; and $^{****}p < .0001$.

the vehicle did not significantly change network electrical activity, TETS (1 μM) significantly increased mean firing rate, burst frequency and area under cross correlation—a measure of network synchronicity (Figs. 8D–G, respectively). Addition of MDZ (0.1 μM) or ALLO alone (0.1 μM) in the absence of TETS suppressed normal network activity, significantly reducing both mean firing rate and burst frequency. However, the combination of ALLO + MDZ (0.1 μM each) in the presence of TETS was sufficient to normalize these measures of network ESA to patterns not different from control.

We compared the relative efficacies of combinations of MDZ plus 4 NAS (Figs. 9A–C). Neuronal network responses to the combination of MDZ plus ALLO, GANAX, XJ-42 or ELTAN (0.1/0.1 μM) were normalized to Veh alone. Under these experimental conditions MDZ plus GANAX (MDZ/GANAX) was less efficacious than the combinations of MDZ and the other NAS toward restoring the elevated mean firing rate and mean burst frequency triggered by the presence of TETS ($p < .001$ and 05 for

MDZ/GANAX vs Veh Control; Figs. 9A and 9B). By comparison, the other combinations tested restored these measures to (MDZ/ALLO) or slightly below (MDZ/ELTAN and MDZ/XJ-42) those measured in Veh control (Figs. 9A and 9B). All 4 MDZ/NAS combinations tested restored neuronal network synchronicity (area under the cross correlation) to levels not significantly different from Veh control (Figure 9C).

DISCUSSION

Complex patterns of synchronous and asynchronous Ca^{2+} oscillations encode essential physiological information for both neuronal and glial cells, respectively, spanning early development, maturation and senescence of specific brain regions (de Melo Reis et al., 2020; Lisek et al., 2020; Pal and Tian, 2020; Stefan, 2020). The frequency and amplitude of SCO patterns are tightly regulated in a context-dependent manner, underscoring the ubiquitous second messenger role of Ca^{2+} requiring temporal
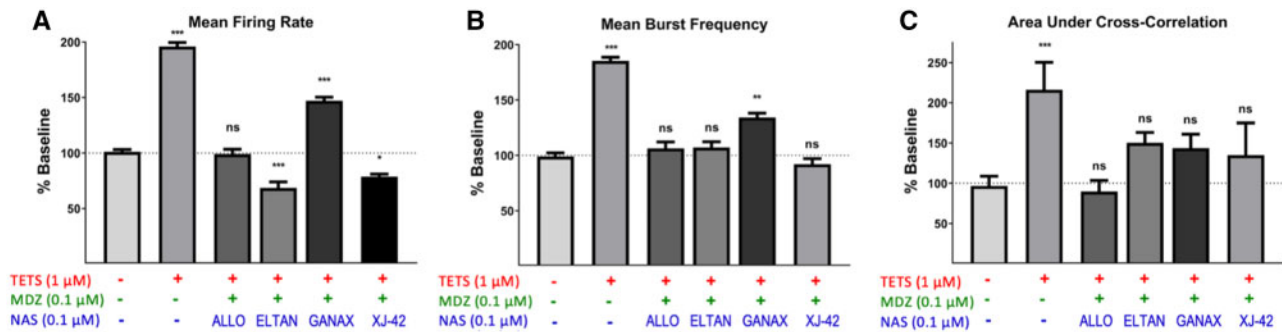
Figure 9. Comparative analysis of 4 neuroactive steroid (NAS) for normalizing tetramethylenedisulfotetramine (TETS)-triggered electrical spike activity (ESA) patterns in the presence of midazolam (MDZ). Mean firing rate (A), mean burst frequency (B) and area under cross correlation (C) of neuronal networks after introducing TETS (1 μM) in the presence of combinations of MDZ (0.1 μM) plus 0.1 μM allopregnanolone, ganaxolone, XJ-42, or eltanolone. ESA events are acquired for 10 min before and after addition of compounds and normalized to their respective baselines. Means of each ESA parameter for each dual intervention were compared with the respective timeframe recorded from Veh control. One-way ANOVA with additional correction (Tukey) for post hoc multiple comparisons are applied to determine the statistical differences. Data represent mean ± SEM of data from 5 to 18 wells. $^*p < .05$; $^{**}p < .01$; $^{***}p < .001$ compared with Veh (no exposure to TETS or MDZ/NAS).

and spatial segregation of meaningful physiological responses (Semyanov *et al.*, 2020). SCO measured from neuronal/glial cocultures recapitulate many developmental and maturation SCO properties measured *in vivo* as they form elaborate functionally interconnected networks that are influenced by seizurogenic agents such as TETS (Cao *et al.*, 2017). Results from the present study are the first to delineate and quantify two distinguishable populations of SCO patterns in neuronal/glial networks cocultured from murine hippocampus. Under the experimental culture conditions used, neuronal networks consistently exhibit characteristic patterns that include more frequent LASE and less frequent HASE patterns during baseline (control) recordings between 14 and 16 DIV. Addition of the GABA$_A$ receptor blocker TETS at concentrations ≥1 μM stabilize HASE while reducing LASE and also significantly increasing the frequency of electrical spikes, bursts and their synchronicity within the neuronal network detected by MEA. Both of these measured outcomes are reflective of hyperexcitation of neuronal circuits, and are presumed to reflect TETS-triggered electrogenic seizure activity measured *in vivo* (Zolkowska *et al.*, 2012, 2018). The present results indicate that patterns of LASE and HASE triggered by TETS may provide a refined quantitative measure for predicting and optimizing novel therapeutic interventions for mitigating TETS-triggered seizure severity while minimizing off target effects. It should be noted that HASE and LASE have distinct influences when expressed as overall mean SCO frequency and amplitude because HASE are of much higher amplitude than LASE. Changes in HASE greatly influences the overall mean SCO amplitude. Since both HASE and LASE are measured simultaneously as averaged fluorescence units across the entire microscopic field in each well, unfortunately we cannot discriminate whether HASE and LASE emanate from all neurons within the network being imaged, or alternatively, from two or more distinct subpopulations of neurons producing SCOs of differing amplitudes. Previous work published from our laboratory focused on the ability of TETS to stabilize HASE, but did not quantify LASE since threshold parameters for counting events were set in a manner that digitally filtered out LASE using postacquisition software (Cao *et al.*, 2012a,b). For example, the combination of ALLO and a benzodiazepine (diazepam) have been shown to be more effective than either drug alone, both *in vitro* (Cao *et al.*, 2012a,b) and *in vivo* (Bruun *et al.*, 2015), however the former *in vitro* studies only assessed influences on total SCO activity, not recognizing LASE as a physiologically relevant *in vitro* biomarker of neuronal network activity.

Separating LASE and HASE when analyzing drugs with distinct primary mechanisms is highlighted by MDZ and PERAMP. Although both drugs suppress HASE and total SCO amplitude, albeit within distinct concentration ranges, their influences on LASE differ as shown in Figure 4. Moreover, a study of seizurogenic agents having distinct chemistry and primary modes of action have been shown to differentially alter SCO patterns *in vitro* (Cao *et al.*, 2015). Thus, the aim of this study was to determine whether 5 chemically related NAS differentially mitigate HASE and LASE patterns triggered by TETS and whether they impact synergistic interactions with MDZ, since the latter was recently adopted as the new standard of care for treating threat-agent induced seizures (Jett and Spriggs, 2018).

This approach leads to the following conclusions: (1) TETS selectively suppresses LASE while stabilizing HASE, and this pattern is coincident with changes in network ESA patterns that have increased spike frequency, increased bursts frequency, and higher synchronicity; (2) of the 5 NAS tested subsequent to establishing the TETS SCO patterns, only ALLO normalizes network activity by stabilizing the LASE pattern without augmenting the frequency of HASE throughout the concentration range tested, a pattern clearly observed with the other NAS tested; (3) MDZ (1–30 μM) reciprocally suppresses HASE while increasing LASE in a concentration dependent manner, although >10 μM greatly suppressed all SCO activity; and (4) the combination of ALLO and MDZ confers significantly more effective control of TETS-triggered SCO and ESA patterns at concentrations less effective with either drug alone (Cao *et al.*, 2012a,b). In the latter regard, evidence of synergistic seizure protection between combinations of NAS and benzodiazepine has been demonstrated in both 6 Hz and hippocampus kindling models, synergism that appears to extend to tonic inhibition of dentate gyrus neurons in culture (Chuang and Reddy, 2020).

These inferences raise several points regarding the pathophysiological consequences of TETS-stabilized HASE patterns as measured *in vitro*, their underlying mechanisms and their predictive value in screening for novel therapeutic approaches to treat acute seizures caused by TETS and structurally related cage convulsants. It is well known that SCOs are a ubiquitous means to provide frequency and intensity encoded biological information, not only locally within the cytosol of individual neurons, but also across distances within interconnected neuronal networks. *In vitro* rodent hippocampal networks first display synchronized ESA early in postnatal development in the form of giant depolarizing potentials produced and regulated by

the balance of GABA and glutamate neurotransmission requiring the prolonged activation of Na^+ channels (Ben-Ari et al., 1989). Such ESA were subsequently shown to drive the rise of intracellular Ca^{2+} in an oscillatory manner reflective of HASE reported here (Valeeva et al., 2010; Griguoli and Cherubini, 2017). With network maturation and upregulation in chloride transporter KCC2b, GABA shifts to an inhibitory (hyperpolarizing) neurotransmitter, and both ESA and SCO patterns become more complex, with highly regulated patterns of frequency and amplitude that are temporally and spatially resolved (Griguoli and Cherubini, 2017; Pinto et al., 2016). In this regard, we have shown hippocampal neuronal/glial cocultures recapitulate both morphometric and functional complexity as they develop over 14 DIV, including an inherent shift from HASE to LASE patterns as the neuronal network matures (Cao et al., 2017). Thus, recognizing that TETS stabilizes the HASE pattern at the expense of suppressing LASE patterns that normally predominate in mature hippocampal networks suggests the former is likely driven by abnormal patterns of ESA that include increased mean firing rate, bust duration and enhance network synchrony as we have shown here. We suggest that TETS-triggered SCO and ESA patterns observed in murine hippocampal cultures reflect seizure-like patterns reported with TETS exposures in vivo, and could serve as predictive biomarkers for optimizing therapeutic candidates for seizure mitigation in vivo. It is reasonable to conclude that TETS-triggered HASE and ESA patterns are functionally linked events mediated by synaptic and intrinsic mechanisms that shape synchronous oscillations in hippocampal neurons in culture (Bacci et al., 1999). They can be considered to represent an in vitro model of TETS-triggered seizure-like activity observed in vivo using electrographic recordings in rodents (Shakarjian et al., 2015; Zolkowska et al., 2018) or zebrafish (Bandara et al., 2020) and behavioral seizure scores (Bruun et al., 2015; Lauková et al., 2019; Pessah et al., 2016).

A growing number of signaling molecules have emerged that respond to distinct SCO patterns and those triggered by receptor-evoked Ca^{2+} events at the synapse. These frequency and spatially encoded Ca^{2+} signals specify biochemical responses in context of developmental state (eg, axonal extension and dendrite complexity) as well as physiological demands (eg, balance of excitatory/inhibitory inputs) placed on individual neurons and the networks they form (Kanemaru et al., 2007; Leinekugel et al., 1997; Pinto et al., 2016; Sharma and Parameswaran, 2018; Smedler and Uhlén, 2014; Tang et al., 2003). It should be emphasized that Ca^{2+} dependent mechanisms of TETS-triggered dysfunction are likely to extend to resident glia in the cultures used in our experiments, which are in contact with the neuronal network. Recently, Nikolic et al. (2020) reviewed the extensive evidence that aberrant astrocyte signaling to neurons contributes to network hyperexcitability, while underscoring the importance of purinergic signaling in regulating neuron-glia and glia-glia Ca^{2+} dynamics both physiologically and in their contribution to dysfunction associated with seizure. Further investigation into how TETS and related cage convulsants influence such cellular interactions seems warranted given the data presented here.

The SAR toward normalizing TETS-triggered SCO patterns reveals that among the 5 closely related NAS congeners tested, only ALLO normalizes HASE while stabilizing LASE throughout the concentration range tested. Moreover, ALLO establishes this HASE/LASE pattern without significantly suppressing total SCO frequency or amplitude below that measured during the same period in control. In contrast, ELTAN the conformational isomer

of ALLO at the 5 position (3α-hydroxy-5β-pregnan-20-one vs 3α-hydroxy-5α-pregnan-20-one, respectively) selectively enhances HASE frequency above that observed with TETS alone without stabilizing LASE. Only at concentrations >1 μM does ELTAN suppress HASE and increase LASE, concentrations that suppress overall network activity compared with the respective control. In fact, the bell-shaped concentration-effect relationship for HASE frequency observed with ELTAN is also mirrored by GANAX and XJ-42, whereas ALPHAX only suppresses HASE significantly at >1 μM (ie, does not enhance HASE at any concentration tested).

The different patterns exhibited by ALLO and ELTAN do not appear to stem from differential potency or efficacy in their functions as PAMs when assessed for GABA-activated Cl^- currents of either $\alpha_1\beta_2\gamma_2$ or $\alpha_2\beta_3\gamma_2$ GABA_ARs composition expressed in heterologous models. However, the differing spatial orientation of the A and B rings of the steroid system, cis in ALLO versus trans in ELTAN introducing a "kink" in the steroid core (Supplementary Figure 1), may confer subtle differences in their activities toward extrasynaptic GABA_AR expressed within the primary neuronal network model implemented here. In support of this possibility, differential interactions with GABA_AR have been identified in recent results from photoaffinity-labeling studies (Jayakar et al., 2020) and are in line with previous reports using biochemical measurements of [^{35}S]TBPS radioligand-receptor binding analyses and membranes isolated from bovine hippocampus (Hawkinson et al., 1994). Despite its similar physicochemical properties, cortisol has virtually no ability to mitigate TETS-triggered SCO patterns. This is consistent with the lack of any known direct actions of cortisol at GABA_AR and further supports our interpretation of a stringent SAR among NAS active through GABA_ARs within the context of the neuronal network model. However, it is also likely that other mechanisms not directly related to their PAM interaction sites on GABA_AR are contributing to differences observed between whole-cell voltage clamp and the more complex Ca^{2+} imaging approaches in primary neuronal networks. Specifically, NAS have also been demonstrated to differentially influence neuronal Ca^{2+} entry dynamics by effects which can promote or diminish voltage-dependent and independent Ca^{2+} entry pathways in a manner that can be stereospecific and dependent on neuronal cell type (Dayanithi and Tapia-Arancibia, 1996; French-Mullen and Spence, 1991; Meyer et al., 2019; Pathirathna et al., 2005; Wang and Brinton, 2008). In this regard, the augmentation of TETS-triggered HASE frequency may serve as a sensitive biomarker for identifying new interventions with improved therapeutic efficacy. Considering the essential contribution of AMPA receptor activity in mediating TETS-triggered SCO patterns demonstrated here and the critical role of synaptic AMPA receptors implicated in promotion and termination of prolonged seizures of status epilepticus (Joshi and Kapur, 2018), the lack of HASE potentiation uniquely observed with ALLO may distinguish ALLO as a candidate of choice to achieve therapeutic efficacy for TETS intoxication. In this regard, NAS, including ALLO, not only elicit PAM activity at GABA_AR subtypes located within synaptic and extrasynaptic regions, but also at axo-somatic, axo-dendritic, and axo-axonal sites within neural networks (Contreras et al., 2019; Olsen, 2018; Lee and Maguire, 2014; Carver and Reddy, 2013). In contrast, the pharmacological responses of benzodiazepines are largely restricted to GABA_AR subunit compositions localized at synaptic sites (Löscher, 2015; Luo et al., 2013). These differences may not only contribute to their distinct pharmacological activities toward mitigating TETS-triggered SCO

patterns, but may also contribute to the greater efficacy when administered in combination with a benzodiazepine. Pressly et al. (2018), using heterologous expression of defined GABA$_A$R subunits, demonstrated that TETS preferentially blocks GABA-activated Cl$^-$ current from channels comprised α_2/β_3 or α_6/β_3 subunits and this may also contribute to differences in activity observed among the NAS tested.

Diazepam and ALLO administered individually at low concentrations have been shown to be ineffective toward rescuing TETS-triggered SCO activity in vitro (Cao et al., 2012a) or TETS-triggered seizures in vivo (Bruun et al., 2015). However, ALLO in combination with diazepam administered subsequent to TETS at concentrations ineffective individually are effective at mitigating TETS-triggered seizure-like activity in vitro and in vivo (Bruun et al., 2015; Cao et al.2012a). Here, we show the response of combinations of MDZ with 4 NAS indicating that the benefits of dual therapy may not extend generally to all NAS, especially at low to intermediate concentrations. The results indicate that only ALLO at low concentration reverses TETS-triggered HASE patterns, whereas the other NAS tested either potentiate HASE in a bell-shaped manner (ELTAN, GANAX, and XJ-42) or only attenuate HASE at high concentration (ALPHAX). TETS exposure rebalances HASE: LASE toward a predominant HASE neuronal network profile, which can serve as an in vitro biomarker of TETS-triggered excitotoxicity and identifying more effective intervention of seizures and possibly treatment of neuropathologic sequelae. The benefits of other modes of combination therapy including diazepam and the NMDA blocker MK801 have been demonstrated to have efficacy in an in vivo mouse model of TETS-induced status epilepticus (Shakarjian et al., 2015). Recently, Lumley et al. (2019) reported that administration of ELTAN (ie, pregnanolone) as an adjunct to diazepam therapy offers additional protection to treat benzodiazepine-refractory status epilepticus, as frequently occurs following delayed treatment of the nerve agent sarin (Lumley et al., 2019). The study also provided strong evidence that dual therapy not only reduces seizure activity, but also performance deficits and brain pathology following exposure to sarin (Lumley et al., 2019), likely a result of marked synergism between benzodiazepine and NAS (Chuang and Reddy, 2020). In this regard, we further demonstrate that ALLO and MDZ in combination confer significant efficacy toward normalizing TETS-triggered SCO and ESA patterns at concentrations ineffective when either are used individually (Cao et al, 2012a).

Based on our results from in vitro analysis of interventions to ameliorate TETS-triggered SCO and ESA patterns, we posit that ALLO remains among the promising leads as a novel antiseizure intervention singly or in combination with the current standard of care, the benzodiazepine MDZ (Jett and Spriggs, 2018). Should our current predictions from in vitro approaches translate to therapeutic efficacy for seizure mitigation and neuroprotection with additional in vivo models of threat agent exposures, the combination of neurosteroid plus benzodiazepine could serve as a generalizable first-line therapeutic approach for anticonvulsant therapy for situations where the threat agent is unidentified or multiple threat agents are suspected.

SUPPLEMENTARY DATA

Supplementary data are available at Toxicological Sciences online.

DECLARATION OF CONFLICTING INTERESTS

I.N.P. is a named inventor of a patent assigned to the Regents of the University of California that is relevant to the work described here. Named inventors of patents and patent applications assigned to the Regents of the University of California that is relevant to the work described here.

REFERENCES

Bacci, A., Verderio, C., Pravettoni, E., and Matteoli, M. (1999). Synaptic and intrinsic mechanisms shape synchronous oscillations in hippocampal neurons in culture. Eur. J. Neurosci. 11, 389–397.

Bandara, S. B., Carty, D. R., Singh, V., Harvey, D. J., Vasylieva, N., Pressly, B., Wulff, H., and Lein, P. J. (2020). Susceptibility of larval zebrafish to the seizurogenic activity of GABA type A receptor antagonists. Neurotoxicology 76, 220–234.

Barrueto, F., Furdyna, P. M., Hoffman, R. S., Hoffman, R. J., and Nelson, L. S. (2003a). Status epilepticus from an illegally imported Chinese rodenticide: "tetramine". J. Toxicol. Clin. Toxicol. 41, 991–994.

Barrueto, F., Nelson, L. S., and Hoffman, R. S. (2003b). Poisoning by an illegally imported Chinese rodenticide containing tetramethylenedisulfotetramine-New York City, 2002. MMWR Morb. Mortal Wkly. Rep. 52, 199–201. Available at: https://www.cdc.gov/mmwr/preview/mmwrhtml/mm5210a4.htm.

Ben-Ari, Y., Cherubini, E., Corradetti, R., and Gaiarsa, J. L. (1989). Giant synaptic potentials in immature rat CA3 hippocampal neurones. J. Physiol. 416, 303–325.

Biffi, E., Regalia, G., Menegon, A., Ferrigno, G., and Pedrocchi, A. (2013). The influence of neuronal density and maturation on network activity of hippocampal cell cultures: A methodological study. PLoS One 8, e83899.

Björklund, U., Persson, M., Rönnbäck, L., and Hansson, E. (2010). Primary cultures from cerebral cortex and hippocampus enriched in glutamatergic and GABAergic neurons. Neurochem. Res. 35, 1733–1742.

Bradley, J. A., Luithardt, H. H., Metea, M. R., and Strock, C. J. (2018). In vitro screening for seizure liability using microelectrode array technology. Toxicol. Sci .163, 240–253.

Bradley, J. A., and Strock, C. J. (2019). Screening for neurotoxicity with microelectrode array. Curr. Protoc. Toxicol. 79, e67.

Bruun, D. A., Cao, Z., Inceoglu, B., Vito, S. T., Austin, A. T., Hulsizer, S., Hammock, B. D., Tancredi, D. J., Rogawski, M. A., Pessah, I. N., et al. (2015). Combined treatment with diazepam and ALLOP regnanolone reverses tetramethylenedisulfotetramine (TETS)-induced calcium dysregulation in cultured neurons and protects TETS-intoxicated mice against lethal seizures. Neuropharmacology 95, 332–342.

Cao, Z., Hammock, B. D., McCoy, M., Rogawski, M. A., Lein, P. J., and Pessah, I. N. (2012a). Tetramethylenedisulfotetramine alters Ca2+ dynamics in cultured hippocampal neurons: Mitigation by NMDA receptor blockade and GABAA receptor-positive modulation. Toxicol. Sci. 130, 362–372.

Cao, Z., Hulsizer, S., Tassone, F., Tang, H. T., Hagerman, R. J., Rogawski, M. A., Hagerman, P. J., and Pessah, I. N. (2012b). Clustered burst firing in FMR1 premutation hippocampal neurons: Amelioration with ALLOP regnanolone. *Hum. Mol. Genet.* **21**, 2923–2935.

Cao, Z., Zou, X., Cui, Y., Hulsizer, S., Lein, P. J., Wulff, H., and Pessah, I. N. (2015). Rapid throughput analysis demonstrates that chemicals with distinct seizurogenic mechanisms differentially alter Ca^{2+} dynamics in networks formed by hippocampal neurons in culture. *Mol. Pharmacol.* **87**, 595–605.

Cao, Z., Xu, J., Hulsizer, S., Cui, Y., Dong, Y., and Pessah, I. N. (2017). Influence of tetramethylenedisulfotetramine on synchronous calcium oscillations at distinct developmental stages of hippocampal neuronal cultures. *Neurotoxicology* **58**, 11–22.

Carver, C. M., and Reddy, D. S. (2013). Neurosteroid interactions with synaptic and extrasynaptic GABAA receptors: Regulation of subunit plasticity, phasic and tonic inhibition, and neuronal network excitability. *Psychopharmacology* **230**, 151–188.

Chuang, S. H., and Reddy, D. S. (2020). Isobolographic analysis of antiseizure activity of the GABA type A receptor-modulating synthetic neurosteroids brexanolone and ganaxolone with tiagabine and midazolam. *J. Pharmacol. Exp. Ther.* **372**, 285–298.

Colombi, I., Mahajani, S., Frega, M., Gasparini, L., and Chiappalone, M. (2013). Effects of antiepileptic drugs on hippocampal neurons coupled to micro-electrode arrays. *Front. Neuroeng.* **6**, 10.

Contreras, A., Hines, D. J., and Hines, R. M. (2019). Molecular specialization of GABAergic synapses on the soma and axon in cortical and hippocampal circuit function and dysfunction. *Front. Mol. Neurosci.* **12**, 154.

Covey, D. F., and Jiang, X. (2014). Inventors, Washington University, assignee. Neuroactive 13,24-cyclo-18,21-dinorcholanes and structurally related pentacylic steroids. U.S. Patent 8,759,330.

Croddy, E. (2004). Rat poison and food security in the People's Republic of China: Focus on tetramethylene disulfotetramine (tetramine). *Arch. Toxicol.* **78**, 1–6.

Dayanithi, G., and Tapia-Arancibia, L. (1996). Rise in intracellular calcium via a nongenomic effect of allopregnanolone in fetal rat hypothalamic neurons. *J. Neurosci.* **16**, 130–136.

de Melo Reis, R. A., Freitas, H. R., and de Mello, F. G. (2020). Cell calcium imaging as a reliable method to study neuron-glial circuits. *Front. Neurosci.* **14**, 569361.

Falk-Petersen, C. B., Søgaard, R., Madsen, K. L., Klein, A. B., Frølund, B., and Wellendorph, P. (2017). Development of a robust mammalian cell-based assay for studying recombinant α_4 $\beta_{1/3}$ δ GABA$_A$ receptor subtypes. *Basic Clin. Pharmacol. Toxicol.* **121**, 119–129.

Frank, C. L., Brown, J. P., Wallace, K., Mundy, W. R., and Shafer, T. J. (2017). Developmental neurotoxicants disrupt activity in cortical networks on microelectrode arrays: Results of screening 86 compounds during neural network formation. *Toxicol. Sci.* **160**, 121–135.

French-Mullen, J. M., and Spence, K. T. (1991). Neurosteroids block Ca^{2+} channel current in freshly isolated hippocampal CA1 neurons. *Eur. J. Pharmacol.* **202**, 269–272.

Griguoli, M., and Cherubini, E. (2017). Early correlated network activity in the hippocampus: Its putative role in shaping neuronal circuits. *Front. Cell Neurosci.* **11**, 255.

Hawkinson, J. E., Kimbrough, C. L., McCauley, L. D., Bolger, M. B., Lan, N. C., and Gee, K. W. (1994). The neuroactive steroid 3 alpha-hydroxy-5 beta-pregnan-20-one is a two-component modulator of ligand binding to the GABAA receptor. *Eur. J. Pharmacol.* **269**, 157–163.

Jayakar, S. S., Chiara, D. C., Zhou, X., *et al.* (2020). Photoaffinity labeling identifies an intersubunit steroid-binding site in heteromeric GABA type A (GABA$_A$) receptors. *J. Biol. Chem.* **295**, 11495–11512.

Jett, D. A., and Spriggs, S. M. (2018). Translational research on chemical nerve agents. *Neurobiol. Dis.* pii:S0969–9961, 30751–30754.

Joshi, S., and Kapur, J. (2018). Mechanisms of status epilepticus: α-Amino-3-hydroxy-5-methyl-4-isoxazolepropionic acid receptor hypothesis. *Epilepsia* **59**(Suppl. 2), 78–81.

Kanemaru, K., Okubo, Y., Hirose, K., and Iino, M. (2007). Regulation of neurite growth by spontaneous Ca^{2+} oscillations in astrocytes. *J. Neurosci.* **27**, 8957–8966.

Koga, K., Iwahori, Y., Ozaki, S., and Ohta, H. (2010). Regulation of spontaneous Ca^{2+} spikes by metabotropic glutamate receptors in primary cultures of rat cortical neurons. *J. Neurosci. Res.* **88**, 2252–2262.

Lauková, M., Velíšková, J., Velíšek, L., and Shakarjian, M. P. (2020). Tetramethylene-disulfotetramine neurotoxicity: What have we learned in the past 70years? *Neurobiol. Dis.* **133**, 104491.

Lauková, M., Pervez, S., Rosman, R., Velíšková, J., Velíšek, L., and Shakarjian, M. P. (2019). Mouse model of human poisonings with tetramethylenedisulfotetramine: Characterization of the effect of exposure route on syndrome outcomes. *Toxicol. Lett.* **308**, 50–55.

Lee, V., and Maguire, J. (2014). The impact of tonic GABAA receptor-mediated inhibition on neuronal excitability varies across brain region and cell type. *Front. Neural Circuits* **8**, 3.

Leinekugel, X., Medina, I., Khalilov, I., Ben-Ari, Y., and Khazipov, R. (1997). Ca^{2+} oscillations mediated by the synergistic excitatory actions of GABA(A) and NMDA receptors in the neonatal hippocampus. *Neuron* **18**, 243–255.

Li, Y., Gao, Y., Yu, X., Peng, J., Ma, F., and Nelson, L. (2014). Tetramine poisoning in China: Changes over a decade viewed through the media's eye. *BMC Public Health* **14**, 842.

Lisek, M., Zylinska, L., and Boczek, T. (2020). Ketamine and calcium signaling-A crosstalk for neuronal physiology and pathology. *Int. J. Mol. Sci.* **21**, 8410.

Löscher, W. (2015). Single versus combinatorial therapies in status epilepticus: Novel data from preclinical models. *Epilepsy Behav.* **49**, 20–25.

Lumley, L., Miller, D., Muse, W. T., Marrero-Rosado, B., de Araujo Furtado, M., Stone, M., McGuire, J., and Whalley, C. (2019). Neurosteroid and benzodiazepine combination therapy reduces status epilepticus and long-term effects of whole-body sarin exposure in rats. *Epilepsia Open* **4**, 382–396.

Luo, R., Partridge, J. G., and Vicini, S. (2013). Distinct roles of synaptic and extrasynaptic GABAAreceptors in striatal inhibition dynamics. *Front. Neural Circuits* **7**, 186.

Massobrio, P., Tessadori, J., Chiappalone, M., and Ghirardi, M. (2015). In vitro studies of neuronal networks and synaptic plasticity in invertebrates and in mammals using multielectrode arrays. *Neural Plast.* **2015**, 1–18.

McConnell, E. R., McClain, M. A., Ross, J., Lefew, W. R., and Shafer, T. J. (2012). Evaluation of multi-well microelectrode arrays for neurotoxicity screening using a chemical training set. *Neurotoxicology* **33**, 1048–1057.

Meyer, L., Taleb, O., Patte-Mensah, C., and Mensah-Nyagan, A. G. (2019). Neurosteroids and neuropathic pain management:

Basic evidence and therapeutic perspectives. *Front. Neuroendocrinol.* **55**, 100795.

Moult, P. R. (2009). Neuronal glutamate and GABAA receptor function in health and disease. *Biochem. Soc. Trans.* **37**(Pt 6), 1317–1322.

Nik, A. M., Pressly, B., Singh, V., Antrobus, S., Hulsizer, S., Rogawski, M. A., Wulff, H., and Pessah, I. N. (2017). Rapid throughput analysis of GABA$_A$ receptor subtype modulators and blockers using DiSBAC$_1$(3) membrane potential red dye. *Mol. Pharmacol.* **92**, 88–99.

Nikolic, L., Nobili, P., Shen, W., and Audinat, E. (2020). Role of astrocyte purinergic signaling in epilepsy. *Glia* **68**, 1677–1691.

Niquet, J., Baldwin, R., Suchomelova, L., Lumley, L., Naylor, D., Eavey, R., and Wasterlain, C. G. (2016). Benzodiazepine-refractory status epilepticus: Pathophysiology and principles of treatment. *Ann. N. Y. Acad. Sci.* **1378**, 166–173.

Nusser, Z. (2016) Subcellular distributions of ligand- and voltage-gated ion channels. In *Dendrites*, 3rd ed. (G. Stuart, N. Spruston, and M. Hausser, Eds), pp. 191–216. Oxford University Press, New York, NY.

Olsen, R. W. (2018). GABA$_A$ receptor: Positive and negative allosteric modulators. *Neuropharmacology* **136**, 10–22.

Pal, A., and Tian, L. (2020). Imaging voltage and brain chemistry with genetically encoded sensors and modulators. *Curr. Opin. Chem. Biol.* **57**, 166–176.

Pathirathna, S., Brimelow, B. C., Jagodic, M. M., Krishnan, K., Jiang, X., Zorumski, C. F., Mennerick, S., Covey, D. F., Todorovic, S. M., and Jevtovic-Todorovic, V. (2005). New evidence that both T-type calcium channels and GABAA channels are responsible for the potent peripheral analgesic effects of 5alpha-reduced neuroactive steroids. *Pain* **114**, 429–443.

Patocka, J., Franca, T. C. C., Wu, Q., and Kuca, K. (2018). Tetramethylenedisulfotetramine: A health risk compound and a potential chemical warfare agent. *Toxics* **6**, 51.

Pessah, I. N., Rogawski, M. A., Tancredi, D. J., Wulff, H., Zolkowska, D., Bruun, D. A., Hammock, B. D., and Lein, P. J. (2016). Models to identify treatments for the acute and persistent effects of seizure-inducing chemical threat agents. *Ann. N. Y. Acad. Sci.* **1378**, 124–136.

Pinto, M. C., Tonelli, F. M., Vieira, A. L., Kihara, A. H., Ulrich, H., and Resende, R. R. (2016). Studying complex system: Calcium oscillations as attractor of cell differentiation. *Integr. Biol. (Camb.)* **8**, 130–148.

Pressly, B., Vasylieva, N., Barnych, B., Singh, V., Singh, L., Bruun, D. A., Hwang, S. H., Chen, Y. J., Fettinger, J. C., Johnnides, S., *et al.* (2020). Comparison of the toxicokinetics of the convulsants picrotoxin and tetramethylenedisulfo-tetramine (TETS) in mice. *Arch. Toxicol.* **94**, 1995–2007.

Pressly, B., Nguyen, H. M., and Wulff, H. (2018). GABA$_A$ receptor subtype selectivity of the proconvulsant rodenticide TETS. *Arch. Toxicol.* **92**, 833–844.

Reddy, D. S., and Estes, W. A. (2016). Clinical potential of neurosteroids for CNS disorders. *Trends Pharmacol. Sci.* **37**, 543–561.

Rudolph, U., and Knoflach, F. (2011). Beyond classical benzodiazepines: novel therapeutic potential of GABAA receptor subtypes. *Nat. Rev. Drug Discov.* **10**, 685–697.

Semyanov, A., Henneberger, C., and Agarwal, A. (2020). Making sense of astrocytic calcium signals - From acquisition to interpretation. *Nat. Rev. Neurosci.* **21**, 551–564.

Shakarjian, M. P., Ali, M. S., Velíšková, J., Stanton, P. K., Heck, D. E., and Velíšek, L. (2015). Combined diazepam and MK-801 therapy provides synergistic protection from tetramethylenedisulfotetramine-induced tonic-clonic seizures and lethality in mice. *Neurotoxicology* **48**, 100–108.

Sharma, R. K., and Parameswaran, S. (2018). Calmodulin-binding proteins: A journey of 40 years. *Cell Calcium* **75**, 89–100.

Smedler, E., and Uhlén, P. (2014). Frequency decoding of calcium oscillations. *Biochim. Biophys. Acta* **1840**, 964–969.

Stefan, C. J. (2020). Endoplasmic reticulum-plasma membrane contacts: Principals of phosphoinositide and calcium signaling. *Curr. Opin. Cell Biol.* **63**, 125–134.

Tang, F., Dent, E. W., and Kalil, K. (2003). Spontaneous calcium transients in developing cortical neurons regulate axon outgrowth. *J. Neurosci.* **23**, 927–936.

Tukker, A. M., Wijnolts, F. M. J., de Groot, A., and Westerink, R. H. S. (2018). Human iPSC-derived neuronal models for in vitro neurotoxicity assessment. *Neurotoxicology* **67**, 215–225.

Valeeva, G., Abdullin, A., Tyzio, R., Skorinkin, A., Nikolski, E., Ben-Ari, Y., *et al.* (2010). Temporal coding at the immature depolarizing GABAergic synapse. *Front. Cell Neurosci.* **4**, 17.

Wang, J. M., and Brinton, R. D. (2008). Allopregnanolone-induced rise in intracellular calcium in embryonic hippocampal neurons parallels their proliferative potential. *BMC Neurosci.* **9**, S11.

Whitlow, K. S., Belson, M., Barrueto, F., Nelson, L., and Henderson, A. K. (2005). Tetramethylenedisulfotetramine: old agent and new terror. *Ann. Emerg. Med.* **45**, 609–613.

Zhang, Y., Su, M., and Tian, D. P. (2011). Tetramine poisoning: A case report and review of the literature. *Forensic Sci. Int.* **204**, e24–e27.

Zhao, C., Hwang, S. H., Buchholz, B. A., Carpenter, T. S., Lightstone, F. C., Yang, J., Hammock, B. D., and Casida, J. E. (2014). GABAA receptor target of tetramethylenedisulfotetramine. *Proc. Natl. Acad. Sci. U.S.A.* **111**, 8607–8612.

Zhu, C. H., Liu, L., and Liu, Y. (2004). The study of status and advances on tetramine poisoning. *Fa Yi Xue Za Zhi* **20**, 37–39.

Zolkowska, D., Banks, C. N., Dhir, A., Inceoglu, B., Sanborn, J. R., McCoy, M. R., Bruun, D. A., Hammock, B. D., Lein, P. J., and Rogawski, M. A. (2012). Characterization of seizures induced by acute and repeated exposure to tetramethylenedisulfotetramine. *J. Pharmacol. Exp. Ther.* **341**, 435–446.

Zolkowska, D., Wu, C. Y., and Rogawski, M. A. (2018). Intramuscular allopregnanolone and ganaxolone in a mouse model of treatment-resistant status epilepticus. *Epilepsia* **59**, 220–227.